Receptance of a semi-infinite periodic railway track and an equivalent multi-rigid body system for use in truncated track models

Xiaozhen Sheng [1, 2*], Yuanpeng He [1, 2], Songtao Yue [1, 2], David Thompson [3]

1. School of Urban Railway Transportation, Shanghai University of Engineering Science, Shanghai, 201620, China

2. Shanghai Engineering Research Centre of Vibration and Noise Control Technologies for Rail Transit, Shanghai, 201620, China

3. Institute of Sound and Vibration Research, University of Southampton, Southampton SO17 1BJ, UK

*Correspondence author: shengxiaozhen@hotmail.com

Emails:

Xiaozhen Sheng: shengxiaozhen@hotmail.com

Yuanpeng He: 674954626@qq.com

Songtao Yue: 1033778307@qq.com

David Thompson: djt@isvr.soton.ac.uk

Abstract

In many problems involving railway track dynamics, the infinitely long railway track has to be truncated, generating a finite track model. To account for high-frequency vibration, high train speed and the presence of multiple carriages, the track model may need to be very long and demand too great computational effort. Alternative modelling strategies are required so that the length of the track model is limited while it is still sufficiently able to exhibit dynamical characteristics of the infinite track. This may be achieved by dividing the track into three parts, two semi-infinite parts (two semi-infinite tracks) on either side of a central finite track model, treating the semi-infinite parts to be periodic in the unbounded direction and then replacing them with an equivalent multi-rigid body system. The multi-rigid body system may be determined based on the requirement that it provides the same receptance to the track model as the semi-infinite track. This paper is concerned with the calculation of the receptance and the determination of the equivalent system for vertical vibration of the track. The receptance is calculated based on the two semi-infinite tracks joined together as an infinitely long periodic structure subject to specific harmonic loads, in combination with the relationship between the internal forces and displacements of a Timoshenko beam. To estimate the parameters of the equivalent system, the structural layout of the system must be created first. The structural layout is created based on the characteristic frequencies and ‘modes’ of the semi-infinite track. The parameters of the equivalent system are estimated by letting the modal frequencies of the equivalent system be the same as the characteristic frequencies of the semi-infinite track and by minimising the relative difference in receptance between the multi-rigid body system and the semi-infinite track at a set of pre-defined frequencies, including the characteristic frequencies of the semi-

infinite track. The above procedure is demonstrated for a typical high-speed slab track and a typical ballasted track.

Keywords: Finite track model; semi-infinite track; equivalent multi-rigid body system.

1. Introduction

Rail corrugation, wheel polygonization, rolling noise and other issues troubling the railway industry require vehicle/track interaction to be analysed for high frequencies from a few hundred hertz to a few thousand hertz [1]. To account for a non-uniform track section and nonlinearity in the track and vehicle systems, time-domain methods are commonly employed, requiring the infinitely long track to be truncated to become a finite length track model with the end of the rail in the track model being either simply supported [2, 3] or applied with other boundary condition [4]. The length of the track model is required to be large for studies of modern high-speed railways, as explained below, and may demand too much computational effort. The length of the track model should be determined based on the following considerations:

(1) The stiffness of the fastener used for high-speed railway slab tracks is normally much lower than that for ballasted tracks. This results in a low vibration decay rate for the rail, which can be as low as 0.5 dB/m for frequencies above just a few hundred hertz [5]. At these frequencies, for rail vibration to decay by 20 dB, a distance of at least 40 m is required. To ensure that wave reflections at the ends of the track model are negligible, the nearest wheelsets must be at least 40 m away from the ends.

(2) The low vibration decay rate will also enhance interactions between neighbouring wheelsets via the rail [6]. Ideally, the entire train should be considered so that rail-induced interactions between all the wheelsets can be fully taken into account. However, by doing so a too large model is generated. A compromise is to consider just three carriages and to focus on the results (time-histories of various quantities) for the middle one. The distance between the two most separated wheelsets of the three carriages is about 75 m for a typical high-speed train.

(3) To calculate time-histories of length of 1 second, the train will have travelled about 111 m when it runs at 400 km/h.

(4) These time-histories are generated through solving a set of ordinary differential equations of motion of the vehicle/track system numerically with pre-defined initial displacements and velocities at $t = 0$. If the initial displacements and velocities are set to zero, as is commonly done, a transient response will be generated in the vehicle/track system [7], since by setting zero (or homogeneous) initial conditions, the simulation is started with the weights of the vehicles being placed on the track instantaneously at $t = 0$. Due to damping in the vehicle/track system, this impulsive response will

eventually become negligible after the train has travelled a certain distance. This distance increases with train speed. Use of non-homogeneous conditions may ease the problem [8].

Thus, by adding all the lengths or distances estimated above, the track model should be at least 266 m (= 40 + 75 + 111 + 40). Ideally the track should be treated as infinitely long and this is possible if the track is idealised as an infinitely long periodic structure. In fact, based on the theory of periodic structure, the track dynamics have been formulated for a ballasted track [9, 10], a ballasted track with rail dampers [11], a slab track [12] and a ballasted track with the rail modelled using the two-and-half dimensional finite element method (2.5D FEM) [13]. Based on these formulations for periodic tracks, several methods have been developed for wheel-rail interaction, either working in the frequency domain [14], or in the time domain [15-18]. In these wheel-rail interaction methods, the wheel is allowed to move [17], and even rotate [18], at the train speed along the track.

Although designed to be periodic, the periodicity of a constructed track is always broken to some extent by various factors. Vehicle dynamics must be studied not only for a perfect track, but also for an imperfect track (e.g., with failures in fasteners [19]), to take into account the effect of these imperfections on the performance of the system. In such cases, the methods based on the theory of periodic structure can no longer be applied, and a finite track model has to be used, as in Ref. [2]. To account for the infinite length of the track, two methods called the sliding window method are proposed respectively in Ref. [19] and Ref. [20]. In the method proposed in Ref. [19], the vehicle and the rail are stationary while the fasteners/sleepers and the 'roughness strip' move backward at the train speed to mimic the motion of the train. Since now the fasteners/sleepers move backward, the vibration generated in the rail may differ from reality since the motion of the dynamic wheel loads relative to the rail is neglected. The method proposed in Ref. [20] is also termed the sliding window method, but the idea is quite different from the one in Ref. [19]. According to Ref. [20], the track is truncated to a finite length (as if the track were seen through a window of that length) with the rail being hinged at the ends. Vehicle/track interaction is computed for a period of time within which the vehicle arrives at position B_0 at $t = T_0$ (initially it is at position A_0 at $t = 0$) but is still well away from the front end of the track model. Next, keeping the vehicle at B_0, the window moves forward by a distance, resulting in a new track model. The new track model must have an overlap with the previous track model. The position of the vehicle relative to the new track model is A_1. Interaction between the vehicle and the new track model is then computed until the vehicle arrives at position B_1 at $t = T_1$, taking the vibrations at $t = T_0$ of the vehicle and the track in the overlapping part as initial conditions. It can be seen that this is an iteration process, but still requires the track model to be long enough to avoid wave reflection from the ends of the track model.

In Ref. [21], Yang and Thompson established a beam model of railway track with a damped and tapered portion connected to the end of the uniform beam. The tapered portion serves as an acoustic black hole (ABH) [22, 23] to attract waves propagating from the uniform beam, so that the infinite nature of the actual track is mimicked to some extent. The results show that the closer the thickness variation of the tapered portion is to the power-law function of a standard ABH ($h(x) = \alpha x^m$, where $m \geq 2$), the better is it at preventing wave reflection; however, the reflection is still considerable when $k_0 L$ is less than π, where k_0 is the wavenumber of the uniform beam and L is the length of the tapered portion.

In the field of soil-structure interaction, a number of absorbing boundaries (e.g., the perfect matching layer, PML [24-26]) have been developed to create nonreflective boundaries, based on the assumption that no wave reflection mechanism exists in the medium beyond the boundary. However, this assumption is not valid for the track, since each fastener can reflect, as well as transmit, part of the incident wave. The forward and backward waves may interfere with each other, producing resonance phenomena. In addition, the rail is a dispersive structure. Therefore, the absorbing boundaries developed for soil-structure interaction cannot be applied to the track.

If the end of the track model has a mechanism which provides the same boundary condition as that provided by the semi-infinite track, the track model will behave the same way as an infinite track. The mechanism may be created by dividing the track into three parts, two semi-infinite parts (two semi-infinite tracks) on either side of a central finite track model, assuming the semi-infinite parts to be periodic in the unbounded direction and then replacing them with an equivalent multi-rigid body system. The multi-rigid body system must provide approximately the same receptance to the track model as the semi-infinite track for a pre-defined frequency range. This paper is concerned with the calculation of the receptance and the determination of the equivalent system for vertical vibration of the track. It should be acknowledged that, analytical receptance expressions are available for a semi-infinite Euler-Bernouli beam and a semi-infinite Timoshenko beam, either in free condition [27] or on a Winkler foundation [28]. Impedance matrix (the inverse of the matrix gives the receptance matrix) is derived in Ref. [29] for a semi-infinite ballasted track using a finite element representation and based on the response of the infinite track subject to a point harmonic force. The response of the infinite track is determined by applying the Floquet transform technique. However, no equivalent system of the semi-infinite track is discussed in Ref. [29]. Different from Ref. [29], in this paper the receptance is calculated by combining the response of an infinitely long periodic structure subject to specific harmonic loads with the relationship between the internal forces and displacements of a Timoshenko beam.

The paper is organised as follows. Calculation of the response of an infinitely long periodic track to harmonic loads is briefly described in Section 2. The receptance matrix of the semi-infinite track is derived in Section 3. Results for the receptance matrix are produced in Section 4 for a typical slab track. The creation of the structure, and the determination of the parameters, of the equivalent multi-rigid body system are also described in this section with most of the details being put in Appendix A. Results are also produced for a typical ballasted track and presented in Section 5 and Appendix B. A preliminary validation of the equivalent multi-rigid body system of the semi-infinite ballasted track is also presented in this section. The paper is concluded in Section 6.

2. Responses of an infinitely long periodic track to harmonic loads

Responses of an infinitely long periodic track to harmonic loads have been formulated for a ballasted track [9, 10], a ballasted track with rail dampers [11] and a slab track [12]. They are all expressed as integrals with respect to wavenumber. However, in these references, results are produced only for a stationary or moving harmonic point force applied on the rail either vertically or laterally. As shown in Section 3, to determine the receptance of the semi-infinite track, the response of the infinitely long periodic track to a harmonic moment is also needed. For this reason and also for better readability, the formulation presented in Ref. [12] for the slab track is briefly recalled below.

2.1 Description of the track

The track, shown in Fig.1, consists of two rails, rail fastener systems, track slabs, a layer of concrete–asphalt (CA) mortar and a concrete base. The end-to-end coupling between two neighbouring slabs is weak and therefore the ends of the slabs are assumed to be free. This paper is mainly concerned with frequencies at which the vibration of the concrete base is much attenuated compared to rail vibration. In addition to that, the concrete base is normally thicker than the track slab and is continuous in the track direction. Therefore, at these frequencies, the concrete base can be approximated to be a rigid foundation. The length of the slab is denoted by L. The track structure is idealised to be periodic in the track (the x-) direction with the period being L. Fig. 1 also shows the coordinate system. The origin of the x-coordinate is located at the interface between two neighbouring slabs (bays of the periodic system) (it is also at the mid-span of two fasteners). The jth bay, where $j \in (-\infty,\ +\infty)$, is located within $[jL, (j+1)L]$. In each bay there are S rail fasteners connecting the rail and the slab, represented by damped springs. The sth fastener in the 0th bay is located at $x = x_s$, where $0 \le x_s < L$. The sth one in the jth bay is at $x = jL + x_s$.

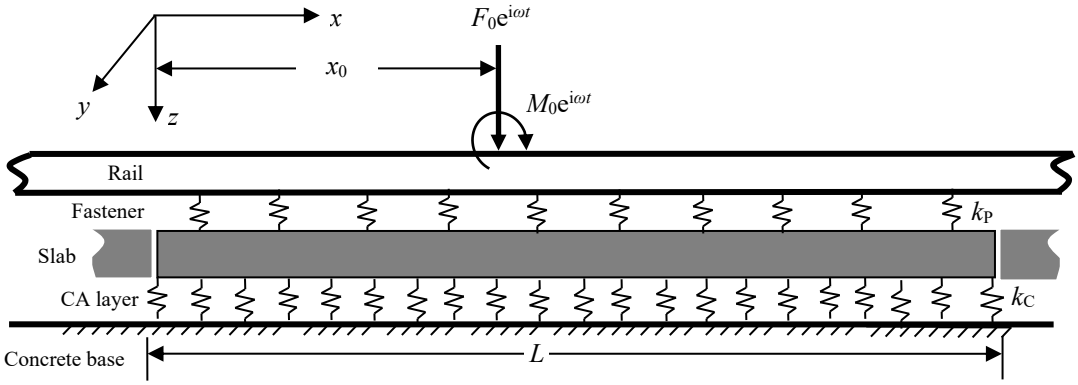

Fig.1. The slab high-speed railway track, the coordinate system and the harmonic loads

2.2 Differential equations of motion of the rail

Only vertical track dynamics is considered in this paper and the vibration is symmetric about the track central plane. For vertical vibration up to about 3000 Hz, the Timoshenko beam theory can be employed to model the rail [30]. According to the Timoshenko beam theory, the differential equation of the rail subject to a vertical harmonic force of amplitude F_0 and a harmonic moment of amplitude M_0 at circular frequency ω, as shown in Fig. 1, is given by [31]

$$\rho A\frac{\partial^2 w}{\partial t^2}-\kappa AG\frac{\partial^2 w}{\partial x^2}+\kappa AG\frac{\partial \psi}{\partial x}=\delta(x-x_0)F_0e^{i\omega t}+\sum_{j=-\infty}^{\infty}\sum_{s=1}^{S}\delta(x-x_s-jL)F_{js}(t), \tag{1}$$

$$\rho I\frac{\partial^2 \psi}{\partial t^2}-EI\frac{\partial^2 \psi}{\partial x^2}-\kappa AG\frac{\partial w}{\partial x}+\kappa AG\psi=\delta(x-x_0)M_0e^{i\omega t}+\sum_{j=-\infty}^{\infty}\sum_{s=1}^{S}\delta(x-x_s-jL)M_{js}(t), \tag{2}$$

where w denotes the vertical displacement (directed downwards) of the rail and ψ is the rotation angle (directed clockwise) of the cross-section of the rail due to bending moment only; x_0 is the location of the harmonic force and moment; $F_{js}(t)$ represents the vertical force (directed downwards) applied to the rail by the sth fastener within the jth slab and $M_{js}(t)$ (directed clockwise) is the moment exerted on the rail in the longitudinal-vertical plane by the fastener; ρ, E, G, A, I and κ are, respectively, the density, Young's modulus, shear modulus, cross-sectional area, second moment of area and shear coefficient of the rail.

2.3 The receptance matrix of a slab at the rail-fastener interfaces within the slab

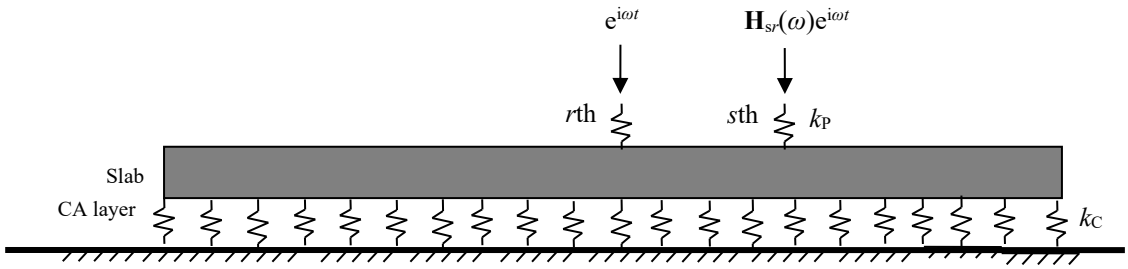

Fig. 2. The receptance corresponding to the responses at the *s*th rail-fastener interface due to excitation at the *r*th rail-fastener interface within a slab

Fasteners on a slab are shown in Fig. 2. The dynamics of the fastener/slab system can be described by a set of receptance matrices associated with the degrees of freedom corresponding to $F_{js}(t)$ and $M_{js}(t)$ (where s = 1, 2, … *S*, see Eqs. (1) and (2)). Since the track is assumed as a periodic structure, these matrices remain the same for all the slabs. The slab is treated as a plate and only the vertical translational vibration is used to couple the fasteners (in other words, the bottoms of the fasteners are assumed to vibrate in the vertical direction only), whereas both the translational and rotational stiffness of the fasteners are taken into account. The 2×2 receptance matrix, corresponding to responses in the degrees of freedom at the *s*th fastener and excitations at the *r*th fastener, is denoted by $\mathbf{H}_{sr}(\omega)$ or $\mathbf{H}_{sr}(f)$. The receptance matrix $\mathbf{H}_{sr}(\omega)$ can be computed from the vertical receptance of the slab and the dynamic stiffness of the fastener. The vertical receptance of the slab is denoted by $G_{sr}(\omega)$, which may be calculated using the finite element method or using a model based on the theory of thin plate and modal superposition. The vertical dynamic stiffness of the fastener is denoted by k_v and the rotational (pitching) dynamic stiffness is denoted by k_φ. Both can be dependent on frequency. Consequently, $\mathbf{H}_{sr}(\omega)$ can be written as

$$\mathbf{H}_{rs}(\omega)=\begin{bmatrix} G_{rs}(\omega)+\delta_{rs}\dfrac{1}{k_v} & 0 \\ 0 & \delta_{rs}\dfrac{1}{k_\varphi} \end{bmatrix}, \tag{3}$$

where δ_{rs} is the Kronecker delta.

2.4 Solution for the displacement of the rail

By letting

$$\mathbf{q}=\begin{Bmatrix} w \\ \psi \end{Bmatrix}, \mathbf{M}=\begin{bmatrix} \rho A & 0 \\ 0 & \rho I \end{bmatrix}, \mathbf{K}_0=\begin{bmatrix} 0 & 0 \\ 0 & \kappa AG \end{bmatrix}, \mathbf{K}_1=\begin{bmatrix} 0 & \kappa AG \\ -\kappa AG & 0 \end{bmatrix}, \mathbf{K}_2=\begin{bmatrix} \kappa AG & 0 \\ 0 & EI \end{bmatrix}, \mathbf{p}_0=\begin{Bmatrix} F_0 \\ M_0 \end{Bmatrix} \tag{4}$$

the steady-state solution of Eq. (1) and Eq. (2) is given by [12]

$$\begin{aligned} \mathbf{q}(x,t)=&\left[\frac{1}{2\pi}\int_{-\infty}^{\infty}[\mathbf{D}(\beta,\omega)]^{-1}\mathrm{e}^{\mathrm{i}\beta(x-x_0)}\mathrm{d}\beta\right. \\ &\left.+\sum_{j=-\infty}^{\infty}\left(-\frac{1}{2\pi L}\mathrm{e}^{-\mathrm{i}2\pi jx/L}\int_{-\infty}^{\infty}[\mathbf{D}(\beta_j,\omega)]^{-1}\mathbf{C}(\beta_j)[\mathbf{A}(\beta)]^{-1}\mathbf{B}(\beta)[\mathbf{D}(\beta,\omega)]^{-1}\mathrm{e}^{\mathrm{i}\beta(x-x_0)}\mathrm{d}\beta\right)\right]\mathbf{p}_0\mathrm{e}^{\mathrm{i}\omega t} \end{aligned}. \tag{5}$$

In Eq. (5),

$$\mathbf{D}(\beta,\omega) = -\omega^2\mathbf{M} + \mathbf{K}_0 + \mathrm{i}\beta\mathbf{K}_1 + \beta^2\mathbf{K}_2, \tag{6}$$

where β is the wavenumber,

$$\mathbf{C}(\beta_j) = \left[\mathrm{e}^{-\mathrm{i}\beta_j x_1}\mathbf{U}_1 \quad \cdots \quad \mathrm{e}^{-\mathrm{i}\beta_j x_S}\mathbf{U}_S \right], \tag{7}$$

where $\beta_j = \beta - 2\pi j/L$ and $\mathbf{U}_s$ is the unit matrix of order 2×2,

$$\mathbf{B}(\beta) = \left[\mathrm{e}^{\mathrm{i}\beta x_1}\mathbf{U}_1 \cdots \mathrm{e}^{\mathrm{i}\beta x_S}\mathbf{U}_S \right]^{\mathrm{T}}, \tag{8}$$

$$\mathbf{A}(\beta) = (\mathbf{A}_{rs}(\beta))_{r,s=1,\cdots S}, \tag{9}$$

where

$$\mathbf{A}_{rs}(\beta) = \mathbf{U}_r^{\mathrm{T}} \left(\frac{1}{L} \sum_{j=-\infty}^{\infty} [\mathbf{D}(\beta_j,\omega)]^{-1} \mathrm{e}^{\mathrm{i}\beta_j (x_r - x_s)} \right) \mathbf{U}_s + \mathbf{H}_{rs}(\omega). \tag{10}$$

Now the observation point is expressed relatively to the load position by setting

$$x' = x - x_0, \tag{11}$$

and Eq. (5) becomes

$$\begin{aligned} \mathbf{q}(x,t) = \Bigg[& \frac{1}{2\pi} \int_{-\infty}^{\infty} [\mathbf{D}(\beta,\omega)]^{-1} \mathrm{e}^{\mathrm{i}\beta x'} \mathrm{d}\beta \\ & + \sum_{j=-\infty}^{\infty} \left(-\frac{1}{2\pi L} \mathrm{e}^{-\mathrm{i}2\pi j(x'+x_0)/L} \int_{-\infty}^{\infty} [\mathbf{D}(\beta_j,\omega)]^{-1} \mathbf{C}(\beta_j) [\mathbf{A}(\beta)]^{-1} \mathbf{B}(\beta) [\mathbf{D}(\beta,\omega)]^{-1} \mathrm{e}^{\mathrm{i}\beta x'} \mathrm{d}\beta \right) \Bigg] \mathbf{p}_0 \mathrm{e}^{\mathrm{i}\omega t} \end{aligned} \tag{12}$$

It can be seen from Eq. (12) that the displacement amplitude of the rail at a given x' is composed of an infinite number of components defined by the index j (the jth term in the infinite sum in Eq. (12)). Each component is expressed as an inverse Fourier transform of a particular function in the wavenumber (β-) domain. Since the track is well damped, the inverse Fourier transform may be performed using the FFT technique for which the integral must be truncated (see Section 4). According to FFT, responses within $|x'| \le x'_{\max}$ will be available, where $x'_{\max} = 2\pi/(2\Delta\beta)$, with $\Delta\beta$ being the wavenumber resolution. For example, if $\Delta\beta = 2\pi \times 0.0025$ rad/m (this value has been shown to be fine enough for normal railway track [9, 11, 12]), then $x'_{\max} = 200$ m. In other words, rail responses within a range of 200 m on either side of the load will be available.

3. Receptance matrix at the end of a semi-infinite periodic track

Now the infinitely long periodic track is cut into two semi-infinite tracks at the junction of two slabs, e.g., the -1th and 0th slabs (i.e., at $x = x_0 = 0$, see Fig. 3). The junction is also at the centre of

the fastener span above these two slabs. This rail cross-section is termed the central cross-section (of the complete track). Consider the right semi-infinite track. At the end a harmonic shear force $\tilde{Q}(\omega)\mathrm{e}^{\mathrm{i}\omega t}$ and a harmonic bending moment $\tilde{M}(\omega)\mathrm{e}^{\mathrm{i}\omega t}$ are applied and the amplitudes of the vertical displacement and rotation angle of the end are denoted by $\tilde{w}(\omega)$ and $\tilde{\psi}(\omega)$. Since the structure is a linear and time-invariant system, the following relation can be written

$$\begin{Bmatrix} \tilde{w}(\omega) \\ \tilde{\psi}(\omega) \end{Bmatrix} = \begin{bmatrix} \alpha_{11}(\omega) & \alpha_{12}(\omega) \\ \alpha_{21}(\omega) & \alpha_{22}(\omega) \end{bmatrix} \begin{Bmatrix} \tilde{Q}(\omega) \\ \tilde{M}(\omega) \end{Bmatrix}, \tag{13}$$

where $\alpha_{ij}(\omega)$ is the receptance of the semi-infinite track at its end (note that $\alpha_{12}(\omega)=\alpha_{21}(\omega)$) and the matrix is the receptance matrix. They can be determined based on the rail responses calculated in Section 2 due to specific harmonic loads, as explained below.

First let a unit vertical harmonic point force be applied on the rail at the central cross-section of the infinite track. The amplitudes of the vertical displacement and the rotation angle of the rail at the cross-section immediately to the right of the load (i.e., at x_0^+) are denoted by $\tilde{w}_1(\omega)$ and $\tilde{\psi}_1(\omega)$, and those of the shear force and bending moment on this cross-section are denoted by $\tilde{Q}_1(\omega)$ and $\tilde{M}_1(\omega)$. It is evident that $\tilde{\psi}_1(\omega)=0$ and $\tilde{Q}_1(\omega)=0.5\,\mathrm{N}$. Then let a unit harmonic moment (in clockwise) be applied. The amplitudes of the vertical displacement and the rotation angle of the rail at the aforementioned cross-section are denoted by $\tilde{w}_2(\omega)$ and $\tilde{\psi}_2(\omega)$, and those of the shear force and bending moment are denoted by $\tilde{Q}_2(\omega)$ and $\tilde{M}_2(\omega)$. It is seen that $\tilde{w}_2(\omega)=0$ and $\tilde{M}_2(\omega)=0.5\,\mathrm{N\cdot m}$. Thus, according to Eq. (13),

$$\begin{bmatrix} \tilde{w}_1(\omega) & 0 \\ 0 & \tilde{\psi}_2(\omega) \end{bmatrix} = \begin{bmatrix} \alpha_{11}(\omega) & \alpha_{12}(\omega) \\ \alpha_{21}(\omega) & \alpha_{22}(\omega) \end{bmatrix} \begin{bmatrix} 0.5 & \tilde{Q}_2(\omega) \\ \tilde{M}_1(\omega) & 0.5 \end{bmatrix},$$

from which the receptance matrix of the semi-infinite track can be worked out

$$\boldsymbol{\alpha}(\omega) = \begin{bmatrix} \alpha_{11}(\omega) & \alpha_{12}(\omega) \\ \alpha_{21}(\omega) & \alpha_{22}(\omega) \end{bmatrix} = \frac{1}{0.25-\tilde{M}_1(\omega)\tilde{Q}_2(\omega)} \begin{bmatrix} 0.5\tilde{w}_1(\omega) & -\tilde{w}_1(\omega)\tilde{Q}_2(\omega) \\ -\tilde{\psi}_2(\omega)\tilde{M}_1(\omega) & 0.5\tilde{\psi}_2(\omega) \end{bmatrix}. \tag{14}$$

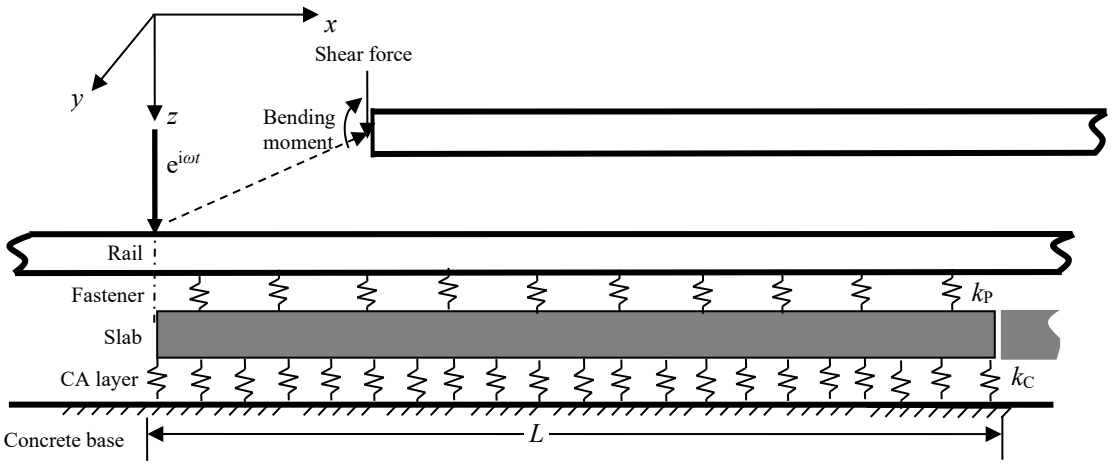

Fig. 3. Shear force and bending moment on the rail cross-section

The shear force and bending moment of the rail appearing in Eq. (14) are related to the displacement of the rail via the following equations [31]

$$M_1(x_0^+,t) = -EI\,\frac{\partial \psi_1(x_0^+,t)}{\partial x}, \tag{15}$$

$$Q_2(x_0^+,t) = -\kappa AG\left(\frac{\partial w_2(x_0^+,t)}{\partial x} - \psi_2(x_0^+,t)\right). \tag{16}$$

Since the rail is subject to a point force or moment, the derivatives of some responses of the rail at the loading cross-section are not uniquely defined according to the beam theory, as shown in Table 1. However, as can be seen from Table 1, all the derivatives appearing in Eqs. (15) and (16) are uniquely defined. These derivatives can be estimated numerically based on $\psi_1(x,t)$ and $w_2(x,t)$ (see Section 4.1for detail).

Table 1. Continuity or discontinuity at x_0 where a point force or moment is applied

$w_1(x,t)$	$\psi_1(x,t)$	$\partial w_1(x,t)/\partial x$	$\partial \psi_1(x,t)/\partial x$
Continuous but not smooth	Continuous and smooth	step	Continuous but not smooth
$w_2(x,t)$	$\psi_2(x,t)$	$\partial w_2(x,t)/\partial x$	$\partial \psi_2(x,t)/\partial x$
Continuous and smooth	Continuous but not smooth	Continuous but not smooth	step

The dynamic stiffness matrix of the semi-infinite track is obtained by inversing $\boldsymbol{\alpha}(\omega)$, i.e.,

$$\boldsymbol{\alpha}^{-1}(\omega) = \begin{bmatrix} 0.5\tilde{w}_1^{-1}(\omega) & \tilde{Q}_2(\omega)\tilde{\psi}_2^{-1}(\omega) \\ \tilde{M}_1(\omega)\tilde{w}_1^{-1}(\omega) & 0.5\tilde{\psi}_2^{-1}(\omega) \end{bmatrix}, \tag{17}$$

and the determinant of the dynamic stiffness matrix is given by

$$\det\left(\boldsymbol{\alpha}^{-1}(\omega)\right)=\frac{0.25-\tilde{M}_1(\omega)\tilde{Q}_2(\omega)}{\tilde{w}_1(\omega)\tilde{\psi}_2(\omega)}. \quad (18)$$

Frequencies at which the determinant reaches a local minimum are characteristic frequencies of the semi-infinite track.

4. The receptance matrix and the equivalent multi-rigid body system for a semi-infinite high-speed slab track

Results for the receptance matrix $\boldsymbol{\alpha}(\omega)$ are produced for a typical high-speed slab track of which the parameters are given in Section 4.1. For this set of parameters, the CA layer is much stiffer than the fastener and the presence of the slab has been found to have negligible effect on the vibration of the rail. Therefore, the results shown below are calculated by treating the slab to be a rigid foundation (however, when the support of the slab is soft (e.g., with a slab mat), the slab should not be treated as a rigid foundation). As a result, the period of the track is now equal to the fastener spacing d. For each bay there is only one fastener, i.e., S = 1. In the calculation, the origin of the x-axis is at the 0th fastener, which, therefore, is at x_1 = 0. Let the point harmonic force and moment be applied at the mid-span of the first bay (this now is the central cross-section of the complete track), i.e., x_0 = 0.5d (see Fig. 1). Results of the infinite track required for calculating the receptances of the semi-infinite track are shown in Section 4.2. Receptances of the semi-infinite track are presented in Section 4.3. The equivalent multi-rigid body system is determined in Section 4.4.

4.1 Parameters of the slab track

The parameters of the track structure are listed in Table 2. They are taken from Ref. [12] but with the railpad stiffness in the vertical direction being adjusted to 5.44×10^7 N/m. The rotational stiffness of the railpad is calculated to be $k_\varphi = k_v b^2/12$, where b is the pad length (0.25 m). Results are evaluated at frequencies from 3 Hz to 3000 Hz with a spacing of 6 Hz. In the calculation, the index j in Eq. (12) is from −20 to 20. Wavenumber is in the range of [$-5000\times0.0025\times2\pi$, $5000\times0.0025\times2\pi$] rad/m (i.e., from -78.5 to 78.5 rad/m) at a spacing of $2\pi\times0.0025$ rad/m. Consequently, the x-spacing is Δx = 0.04 m. As shown in Eq. (14) to Eq. (16), to calculate the receptances of the semi-infinite track, derivatives of the displacements of the infinite track with respect to x are required. The derivatives are computed numerically, as what follows. Since $\psi_1(x,t)$ (the same for $w_2(x,t)$) is anti-symmetric about x_0 (i.e., $\psi_1(x_0,t)=0$ and for any x, $\psi_1(x_0-x,t)=-\psi_1(x_0+x,t)$) , it can be approximated as $a(t)(x-x_0)+b(t)(x-x_0)^3$ around x_0, and $\partial\psi_1(x_0,t)/\partial x=a(t)$. It can be shown that $a(t)$ is given by $(8y_1-y_2)/(6\Delta x)$, where y_1 and y_2 are the values of $\psi_1(x,t)$ at $x_0+\Delta x$ and $x_0+2\Delta x$, respectively. The x-spacing and the way of calculating

the derivatives have been shown to give almost the same results as Timoshenko-beam finite element models (the FE model for the infinite track contains 1000 spans and that for the semi-infinite track contains 500 spans).

Table 2. Parameters for the vertical dynamics of the track

Density of the rail	$\rho = 7850$ kg/m^3
Young's modulus of the rail	$E = 2.1\times10^{11}$ N/m^2
Shear modulus of the rail	$G = 0.81\times10^{11}$ N/m^2
Loss factor of the rail	$\eta_R = 0.01$
Cross-sectional area of the rail	$A = 7.69\times10^{-3}$ m^2
Second moment of area of the rail	$I = 30.55\times10^{-6}$ m^4
Shear coefficient of the rail cross-section	$\kappa = 0.4$
Vertical rail pad stiffness	$k_v = 5.44\times10^7$ N/m
Rotational rail pad stiffness	$k_\varphi = 2.83\times10^5$ N·m/rad
Rail pad loss factor	$\eta_P = 0.1$
Fastener spacing	$d = 0.65$ m

4.2 Results for the complete slab track

In order to determine the receptances of the semi-infinite track, according to Eq. (14), results for the complete track (i.e., $\tilde{w}_1(\omega), \tilde{\psi}_2(\omega), \tilde{Q}_2(\omega), \tilde{M}_1(\omega)$) should be calculated first. They are shown in Fig. 4 from which resonance/anti-resonance phenomena of the track can be seen. Discussion of the vibration behaviour of an infinitely long periodic track can be found in Ref. [32]. The receptance ($\tilde{w}_1(\omega)$) associated with the vertical harmonic point force exhibits peaks at about 183 Hz, 940 Hz and 2607 Hz. The first peak at about 183 Hz is mainly contributed by the bouncing mode of the rail (the frequency may be termed the bouncing frequency which can be simply estimated by $\sqrt{k_V/(\rho A d)}/(2\pi)$). In this mode the rail vibrates vertically like a rigid bar on the fasteners. The second peak is mainly contributed by a mode of the track which is now commonly known as the first pinned-pinned mode. In this mode the cross-sections of the rail at fastener locations rotate only (as if the rail were pinned at the fastener positions) while the mid-span cross-sections vibrate vertically without rotation (i.e., the cross-sections are just sliding vertically). The peak at about 2607 Hz will be discussed later. Due to the excitation of other modes or waves, the actual motions of the track at the peak frequencies differ from the corresponding pure modes of the track.

There are peaks at about 183 Hz and 980 Hz in the receptance ($\tilde{\psi}_2(\omega)$) associated with the harmonic moment. At the first frequency, the rail in the vicinity of the load exhibits an approximate rigid pitching motion about the central cross-section, accompanied with the cut-on of bending waves in the rail beyond the vicinity. Therefore, the frequency may be termed the pitching frequency which is identical to the bouncing frequency. The second peak at about 980 Hz is mainly contributed by another track mode. In this mode, the cross-sections of the rail at any two neighbouring fastener

positions vibrate vertically with the same amplitude but in opposite directions while the mid-span cross-sections vibrate with rotation only. This mode may be termed the sliding-pinned-sliding* mode and the frequency is termed the sliding-pinned-sliding* frequency. Here the three words forming the term are respectively for the left, middle and right cross-sections of the rail in a bay, while the star symbol '*' means that the right cross-section vibrates in the direction opposite to the left one.

As seen in Fig.4, modes are also indicated at about 2577 Hz and 2607 Hz. In the mode at 2577 Hz, all the mid-span cross-sections and all those at fastener positions behave like being pinned. In the literature, this mode is commonly known as the second pinned-pinned mode. In the mode at about 2607 Hz, all the mid-span cross-sections and all those at fastener positions behave like being rotationally blocked, only sliding in the vertical direction. All the mid-span cross-sections slide in the same direction and all those at fastener positions slide in the opposite direction. Hence, the mode and frequency are termed, respectively, the sliding-sliding*-sliding mode and the sliding-sliding*-sliding frequency.

A summary of the vibration characteristics of the complete slab track at the aforementioned frequencies are given in Table 3.

Table 3. Vibration characteristics of the complete slab track

Peak or dip frequency (Hz)	Description of the mode
183	Rail bouncing on the stiffness of the fasteners
940	The first pinned-pinned mode
980	The sliding-pinned-sliding* mode
2577	The second pinned-pinned mode
2607	The sliding-sliding*-sliding mode

Similar discussion can be made about the shear force and the bending moment. The shear force due to the moment excitation exhibits dips at the pitching frequency (183 Hz) and the sliding-pinned-sliding* frequency (980 Hz) while the bending moment due to the force excitation exhibits peaks at the bouncing frequency (183 Hz) and the first pinned-pinned frequency (940 Hz). Also shown in Fig. 4 is the determinant of the dynamic stiffness matrix of the semi-infinite track (see Eq. (18)). A dip appears at the first resonance frequency of the infinite track (i.e., at 183 Hz). This frequency is also a resonance frequency of the semi-infinite track, as will be shown in Section 4.3. The determinant has a peak at the second pinned-pinned frequency (2577 Hz) and a dip at the sliding-sliding*-sliding frequency (2607 Hz). At the first pinned-pinned (940 Hz) and the sliding-pinned-sliding* (980 Hz) frequencies there is only a weak feature.

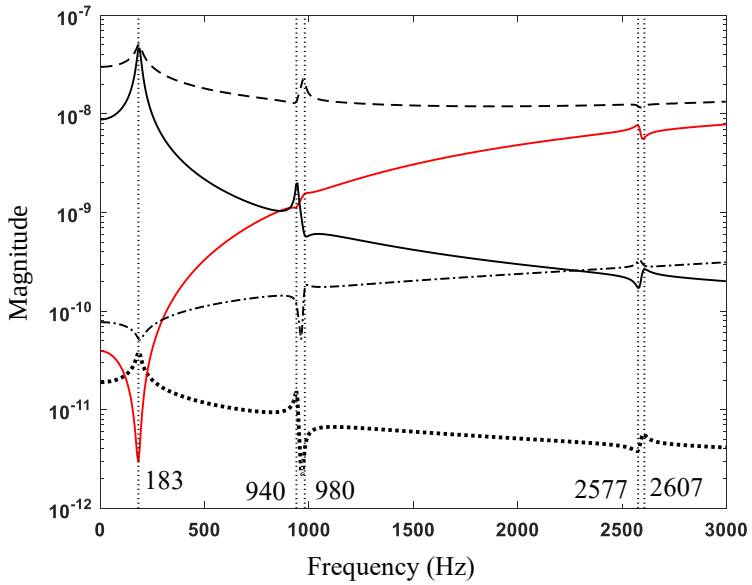

Fig. 4. Results for the complete slab track: —, $\tilde{w}_1(\omega)$ (m/N); – –, $\tilde{\psi}_2(\omega)$ (1/(N·m)); –·–, $\tilde{Q}_2(\omega)\times10^{-10}$ (N/N·m); ……, $\tilde{M}_1(\omega)\times10^{-10}$ (N·m/N); Red, $\det(\boldsymbol{\alpha}^{-1}(\omega))\times10^{-25}$ (N^2)

4.3 Receptances of the semi-infinite slab track

The magnitudes and phases of the receptances at the end of the semi-infinite track are shown in Fig. 5 and Fig. 6. Fig. 5 shows that, all the receptances have a peak at about 183 Hz, of which the correspodning angular frequency is denoted by ω_n. This is related to the bouncing and pitching modes mentioned in Section 4.2, although the end (corresponding to the central cross-section of the complete track) of the semi-infinite track is free while in the complete track the cross-section is constrained by the other semi-infinite track. In addition, as shown in Fig. 5, the receptances of the semi-infinite track also exhibit peaks/dips at other much higher characteristic frequencies (940 Hz, 980 Hz, 2577 Hz and 2606 Hz) of the complete track. At the first pinned-pinned frequency (940 Hz), $|\alpha_{11}|$ exhibits a peak and $|\alpha_{22}|$ exhibits a dip, similar to the infinite track in Fig. 4. At the second pinned-pinned frequency (2577 Hz), $|\alpha_{11}|$ exhibits a dip while $|\alpha_{22}|$ shows a peak.

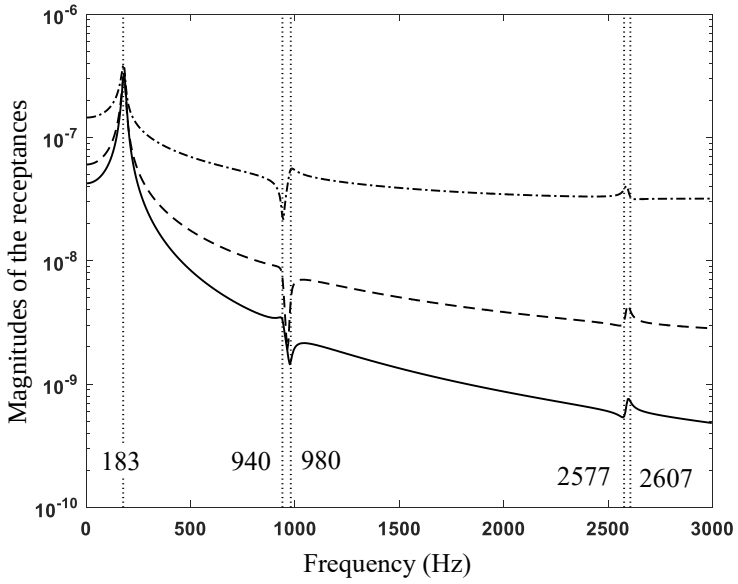

Fig. 5. Magnitudes of the receptances. —, $|\alpha_{11}|$ (m/N); – –, $|\alpha_{12}|$ (1/N); –·–, $|\alpha_{22}|$ (1/(N·m))

Turning to the phases of the receptance shown in Fig. 6, it can be seen that, as frequency reduces to zero, the phases become close to zero or π and the magnitudes shown in Fig. 5 approach the static flexibilities of the semi-infinite track. The static cross-flexibility (i.e., α_{12}) has a phase of about π, consistent with the definitions of the excitation and response for the receptances; from Fig. 3 it can be seen that, the static shear force will cause the rail end to rotate in the anticlockwise direction, opposite to the positive direction of rotation. The phases at 183 Hz are close to either π/2 or –π/2, indicating that the peak shown in Fig. 5 at this frequency can be approximated as a damped modal behaviour. It is interestingly noticed that, at high frequencies, the phase of α_{11} is close to –3π/4 while that of α_{22} is close to –π/4, similar to those at the end of a free Euler beam.

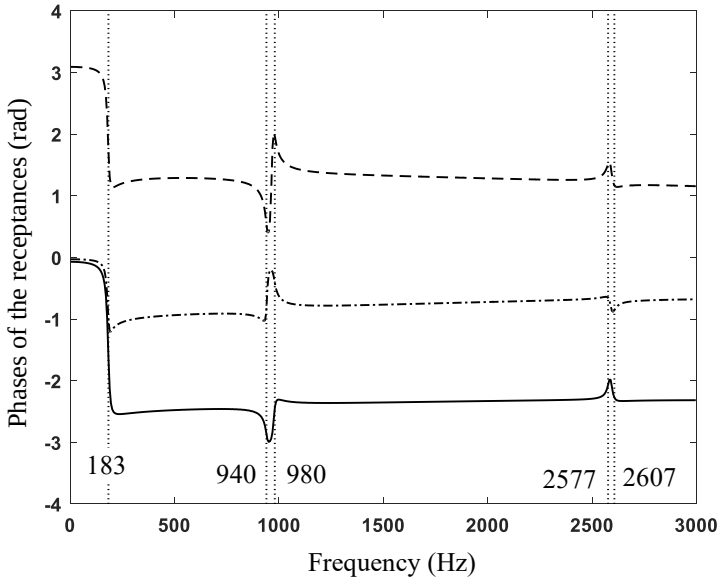

Fig. 6. Phases of the receptances. —, for α_{11}; – –, for α_{12}; –·–, for α_{22}

4.4 The multi-rigid body system equivalent to the semi-infinite slab track

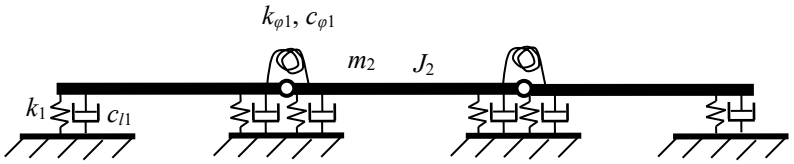

Fig. 7. The multi-rigid body system equivalent to the semi-infinite slab track

One of the purposes of this paper is to determine a multi-rigid body system which is dynamically equivalent to the semi-infinite track. To do so, the layout of the equivalent system must be created first. It is natural to think of a multi-rigid body system which looks geometrically like a track. Thus, as shown in Fig. 7, the equivalent multi-rigid body system is formed of a series of rigid bars hinged together, geometrically looking like a rail. Vertical springs and dampers are attached to the ends of each bar, mimicking the fasteners. Bending springs and dampers are used to connect two neighbouring bars, mimicking the bending stiffness of the rail. The number of the rigid bars is denoted by N. The mass, length and moment of inertia about the centre of mass of the jth bar are denoted by m_j, L_j and J_j, respectively, where $j = 1, 2, \ldots, N$. The stiffnesses of the springs at the two ends of the jth bar are identical and denoted by k_j while the dampers are allowed to have different damping coefficients, with c_{lj} for the left damper and c_{rj} for the right damper. The stiffness of the bending spring connecting the jth and (j+1)th bars is denoted by $k_{\varphi j}$ and the coefficient of the corresponding bending damper is denoted by $c_{\varphi j}$, where $j = 1, 2, \ldots, N$–1.

The next step is to determine the parameters for the equivalent multi-rigid body system so that the receptance at the left end of the multi-rigid body system is close to that of the semi-infinite track for a frequency range. Use is first made of the resonance frequency (i.e., ω_n) in Fig. 5. When the following relationships are satisfied, the first two modal frequencies of the equivalent system are identical to ω_n:

$$k_j = \frac{1}{2} m_j \omega_n^2, \tag{19}$$

$$J_j = \frac{1}{4} m_j L_j^2 \tag{20}$$

Therefore, the parameters that are left to be determined for the equivalent system are m_1, L_1, c_{l1}, c_{r1}, $k_{\varphi 1}, c_{\varphi 1}$, …, m_N, L_N, c_{lN}, c_{rN}. The total number of the unknown parameters is 6N-2.

Now it is assumed that a vertical harmonic force $\tilde{Q}e^{i\omega t}$ (directed downward) and a harmonic moment $\tilde{M}e^{i\omega t}$ (in clockwise) are applied to the first rigid bar at the left end. The vertical

displacement of the left end of the first rigid bar is denoted by $w_1(t) = \tilde{w}_1 e^{i\omega t}$ (directed downward) and the rotation angle of the *j*th bar is denoted by $\varphi_j(t) = \tilde{\varphi}_j e^{i\omega t}$ (directed clockwise). The equivalent system has *N*+1 degrees of freedom defined by $w_1(t), \varphi_1(t), \cdots \varphi_N(t)$. The amplitude vector defined by

$$\tilde{\mathbf{q}}_e = (\tilde{w}_1, \tilde{\varphi}_1, \cdots, \tilde{\varphi}_N)^T, \tag{21}$$

satisfies

$$[-\mathbf{M}_e\omega^2 + i\omega\mathbf{C}_e + \mathbf{K}_e]\tilde{\mathbf{q}}_e = (\tilde{Q}, \tilde{M}, 0, \cdots 0)^T, \tag{22}$$

where $\mathbf{M}_e$, $\mathbf{C}_e$ and $\mathbf{K}_e$ are the mass, damping and stiffness matrices of the multi-rigid body system and they are derived in Appendix A. From Eq. (22), the receptances (translation, rotation and cross) at the left end of the first rigid bar can be determined. By equating the receptances to those of the semi-infinite track at a number, *M*, of pre-selected frequencies (*M* should be greater than or equal to *N*), a set of 6*M* nonlinear equations (3*M* for the real parts of the receptances and the other 3*M* for the imaginary parts) are formed. The equations take the form of $\mathrm{Re}(\alpha_E - \alpha)/|\alpha| = 0$ and $\mathrm{Im}(\alpha_E - \alpha)/|\alpha| = 0$, where α stands for the receptance of the semi-infinite track and α_E stands for that of the equivalent system. From these equations the 6*N*-2 parameters of the equivalent system can be determined using a proper solver (in this paper the Matlab solver 'lsqnonlin' is used). To solve the nonlinear equations, initial values of the unknowns are required. They may be determined based on the parameters of the track; for example, the actual railpad stiffness may be used as the initial value for the stiffness of the end springs of the rigid bars, while the rail mass in one sleeper bay may be taken for the initial value of the masses of the rigid bars.

The equivalent multi-rigid body system created above has *N*+1 natural frequencies. The first two are repeated and equal to ω_n (183 Hz, the first characteristic frequency of the semi-infinite track). For the equivalent system to be able to exhibit receptance curves similar to those of the semi-infinite track at and around ω_n, the receptance of the semi-infinite track must be satisfied at least for three frequencies (one lower than, one equal to, and the other higher than, ω_n), at least giving 18 equations. On the other hand, the equivalent system has a number of 6*N*-2 parameters to be determined. Therefore, *N* must at least be 3. Based on this reasoning, if more characteristic frequencies are considered, *N* must be increased accordingly. Unfortunately, it is still not successful to find a set of parameter values which can make the equivalent system cover frequencies higher than the first pinned-pinned frequency. In other words, the equivalent multi-rigid body system created above seems to work only for frequencies lower than the first pinned-pinned frequency.

The determined parameters of the equivalent system are listed in Table 4 for *N* = 5 and the pre-selected frequencies are 3, 15, 87, 117, 183, 207, 333, 597, 897 Hz (*M* = 9). This number of

frequencies gives a set of 54 equations, much more than the number ($6 \times 5 - 2 = 28$) of the unknown parameters. Since the number of degrees of freedom of the equivalent system is much limited while that of the semi-infinite track is unlimited, the parameters are quite different from bar to bar. The second and fourth bars are massless and the stiffness of the associated spring are zero. Further, the damping coefficients of the two dampers for the fourth bar are also zero. However, the rotational stiffness and damping between the fourth bar and its neighbours are not vanishing. The receptance of the equivalent system and that of the semi-infinite track are compared in Fig. 8 for the magnitudes and Fig. 9 for the phases. The multi-rigid body system matches very well with the semi-infinite track for frequencies up to about 900 Hz.

It is also tested for $N = 3$, 4 and 6 and other numbers of frequencies. However, none of them gives better agreement than those shown in Figs. 8 and 9.

Table 4. Parameters of the mass-spring-damper system equivalent to the semi-slab track

No. of bar	1	2	3	4	5
m (kg)	10.080	0.000	67.013	0.000	257.134
J (kg·m^2)	0.021	0.000	3.104	0.000	0.917
L (m)	0.091	0.329	0.430	0.181	0.119
k (N/m)	0.666×10^7	0.000	4.430×10^7	0.000	16.998×10^7
c_l (N·s/m)	0.000	0.206×10^3	2.876×10^3	0.000	0.000
c_r (N·s/m)	0.206×10^3	2.876×10^3	0.000	0.000	102.930×10^3
k_φ (N·m/rad)	2.099×10^7	1.275×10^7	0.288×10^7	0.061×10^7	
c_φ (N·m·s/rad)	0.321×10^3	2.882×10^3	0.529×10^3	0.792×10^3	

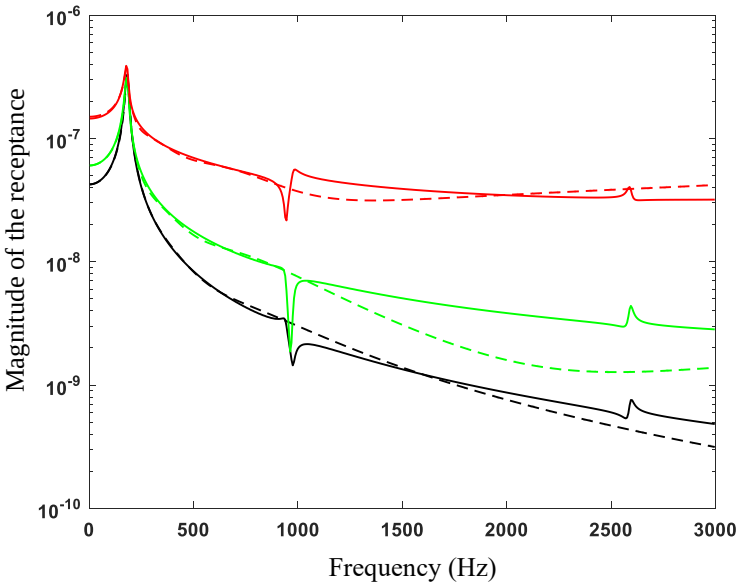

Fig. 8. The magnitudes of the receptances of the semi-infinite slab track (—) and the equivalent system (- - -). Black for α_{11} (m/N), green for α_{12} (rad/N) and red for α_{22} (rad/(N·m))

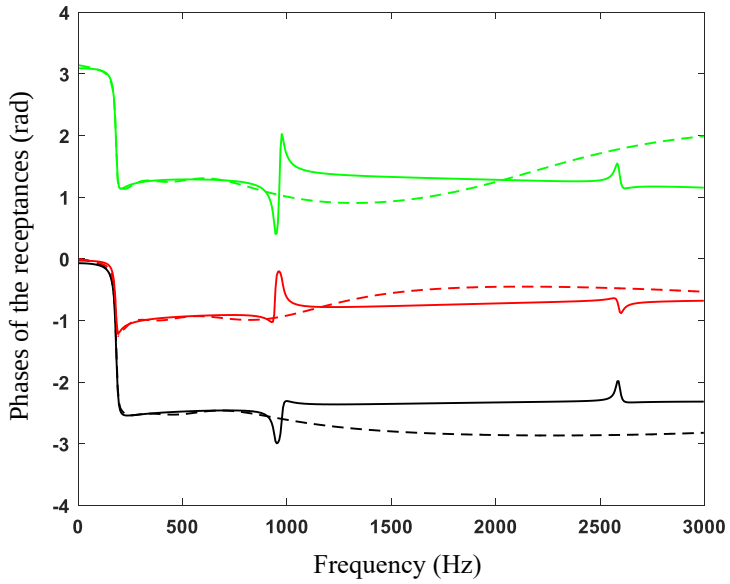

Fig. 9. The phases of the receptances of the semi-infinite slab track (—) and the equivalent system (- - -). Black for α_{11} (m/N), green for α_{12} (rad/N) and red for α_{22} (rad/(N·m))

5. The receptance matrix and the equivalent multi-rigid body system for a semi-infinite ballasted track

In this section, the receptance matrix $\boldsymbol{\alpha}(\omega)$ and the equivalent multi-rigid body system are produced for a typical ballasted track. As in Ref. [9], the sleepers are modelled as rigid bodies and the ballast under sleepers is idealised as springs. The track parameters are given in Table 5. Again, in the calculation, the wavenumber is within [-78.5, 78.5] rad/m at a spacing of $2\pi\times0.0025$ rad/m, the index j in Eq. (12) is from -20 to 20, and frequencies are from 3 Hz to 3000 Hz with a spacing of 6 Hz. Results of the complete ballasted track required for calculating the receptances of the semi-infinite ballasted track are shown in Section 5.1. Receptances and the equivalent multi-rigid body system of the semi-infinite ballasted track are presented in Section 5.2. A preliminary validation of the equivalent system is presented in Section 5.3.

Table 5. Parameters for the vertical dynamics of the ballasted track

Parameters for the rail	As in Table 2
Vertical rail pad stiffness	$k_v = 3.5\times10^8$ N/m
Rotational rail pad stiffness	$k_\varphi = 1.82\times10^6$ N·m/rad
Rail pad loss factor	$\eta_P = 0.1$
Mass of half a sleeper	$m_S = 150$ kg
Sleeper spacing	$d = 0.6$ m
Ballast stiffness	$k_B = 100\times10^6$ N/m
Ballast loss factor	$\eta_B = 0.3$

5.1 Results of the complete ballasted track

Results of $\tilde{w}_1(\omega), \tilde{\psi}_2(\omega), \tilde{Q}_2(\omega), \tilde{M}_1(\omega)$ are shown in Fig. 10. Seven characteristic frequencies of the complete ballasted track are identified in the figure, which are 117 Hz, 243 Hz, 531 Hz, 1077 Hz, 1269 Hz, 2871 Hz and 2955 Hz. A description of the vibration characteristics of the complete ballasted track at these frequencies are given in Table 6. For more discussion, see Ref. [32].

Table 6. Vibration characteristics of the complete ballasted track

Peak or dip frequency (Hz)	Description of the mode
117	Rail and sleeper bouncing together on the ballast
243	Sleeper behaving as vibration absorber to the rail
531	Rail and sleeper bouncing out-of-phase
1077	The first pinned-pinned mode
1269	The sliding-pinned-sliding* mode
2871	The second pinned-pinned mode
2955	The sliding-sliding*-sliding mode

Also shown in Fig. 10 is the determinant of the dynamic stiffness matrix of the semi-infinite ballasted track (see Eq. (18)). Three dips appear at about 117 Hz, 489 Hz and 2925 Hz. These are the resonance frequencies of the semi-infinite ballasted track, as shown in Fig. 11. The first one is identical to the first characteristic (resonance) frequency of the complete ballasted track (see Table 6), while the second is much lower than the second resonance frequency (531 Hz) of the complete track. It is also seen that the determinant has peaks at 243 Hz and 2871 Hz (the second pinned-pinned frequency). At these two frequencies, the receptances of the semi-infinite ballasted track have dips (Fig. 11).

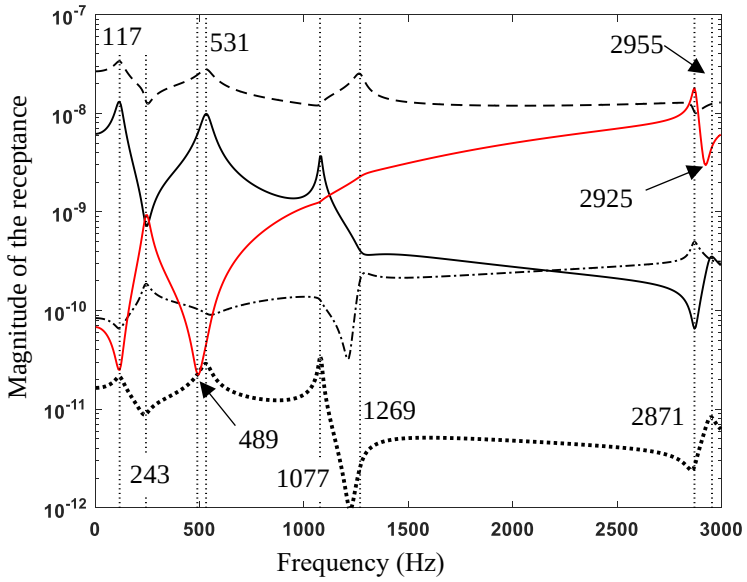

Fig. 10. Results for the complete ballast track. —, $\tilde{w}_1(\omega)$ (m/N); – –, $\tilde{\psi}_2(\omega)$ (1/(N·m)); –·–, $\tilde{Q}_2(\omega)\times 10^{-10}$ (N/N·m); ……, $\tilde{M}_1(\omega)\times 10^{-10}$ (N·m/N); Red, $\det(\boldsymbol{\alpha}^{-1}(\omega))\times 10^{-25}$ (N²)

5.2 Receptances of the semi-infinite ballasted track and the the equivalent multi-rigid body system

The receptances of the semi-infinite ballasted track are shown in Fig. 11. It can be seen that at about 117 Hz, 489 Hz and 2925 Hz, all the three receptances have a peak. The first two frequencies are denoted by ω_{n1} and ω_{n2} (angular frequency), respectively. These peaks can be explained as done in Section 4.3. In other words, the semi-infinite track has repeated modal frequencies at 117 Hz and 489 Hz. All the three receptances have a dip at 243 Hz, which, denoted by ω_{anti}, is an anti-resonance frequency. Note that, both the complete track and the semi-infinite track exhibit resonance at about 117 Hz and anti-resonance at about 243 Hz. This is because these two frequencies are determined mainly by the mass of the sleeper and the stiffnesses of the ballast and railpad, not changing significantly with the constraint condition at the central cross-section of the rail. However, the second resonance frequency of the complete track (531 Hz) is much higher than that of the semi-infinite track (489 Hz). This is because the rail has a great effect on the frequency; it shifts to a lower value when the rail is cut at the central cross-section of the complete track.

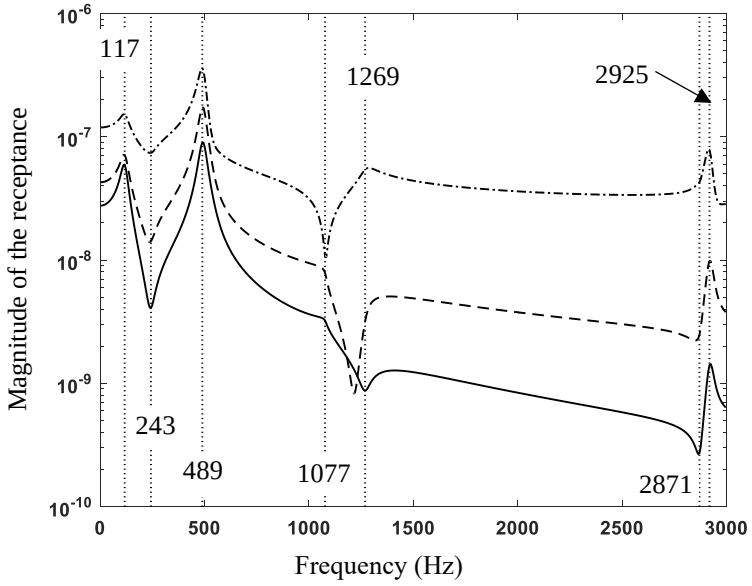

Fig. 11. Magnitudes of the receptances of the semi-infinite ballasted track. —, $|\alpha_{11}|$ (m/N); – –, $|\alpha_{12}|$ (1/N); –·–, $|\alpha_{22}|$ (1/(N·m))

Based on the characteristics of the receptance of the semi-infinite ballasted track, a multi-rigid body system which is dynamically equivalent to the semi-infinite track for a frequency range can be constructed and determined. The layout of the equivalent system is created based on the same idea as for the slab track in Section 4.4. The equivalent multi-rigid body system is shown in Fig. 12. It is formed by a number of N rigid bars hinged together. The mass, length and moment of inertia about the mass centre of the jth bar are denoted by m_j, L_j and J_j, where $j = 1, 2, \ldots, N$. Each end of a bar is supported by a mass-spring-damper system. The stiffnesses of the upper springs at the two ends of

the jth bar are identical and denoted by k_j while the dampers are allowed to have different damping coefficients, with c_{lj} for the left damper and c_{rj} for the right damper. The stiffnesses of the lower springs for the jth bar are also identical and denoted by s_j while the dampers are also allowed to have different damping coefficients, with d_{lj} for the left lower damper and d_{rj} for the right lower damper. The mass is denoted by μ_j for the jth bar (this is termed the support mass of the jth bar). A rotational spring $k_{\varphi j}$ and a rotational damper $c_{\varphi j}$ connect the right end of the jth bar and the left end of the (j+1)th bar, where j = 1, 2, …, N-1. The total number of parameters of the equivalent multi-rigid body system are 12N-2.

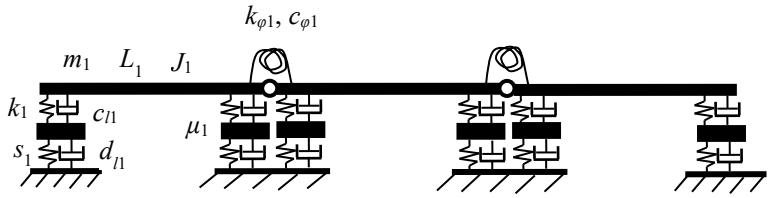

Fig. 12. The multi-rigid body system equivalent to the semi-infinite ballasted track

The next step is to determine the parameters for the equivalent system so that the receptance at the left end of the system is close to that of the semi-infinite track for a frequency range. The frequency range considered in this paper is much higher than ω_{n2} but still well lower than the first pinned-pinned frequency. To determine the parameters, use is first made of the anti-resonance frequency. In other words, the natural frequency of the support mass on the stiffness of the upper and lower springs is required to equal to the anti-resonance frequency, i.e.,

$$\mu_j = (k_j + s_j) / \omega_{\text{anti}}^2 . \tag{23}$$

Secondly, each undamped unit (the jth one is shown in Fig. 13) of the equivalent system is required to have two pairs of repeated natural frequencies, one being ω_{n1} (i.e., 2π×117 rad/s) and the other being ω_{n2} (i.e., 2π×465 rad/s). Since the system shown in Fig. 13 is symmetric, it has two symmetric modes and two anti-symmetric modes. The modal frequencies of the symmetric modes are required to be repeated by the anti-symmetric modes. It can be shown that, the two modal frequencies of the symmetric modes are given by

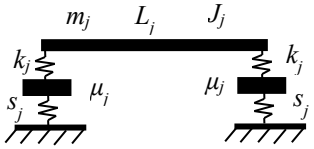

Fig. 13. A unit cell of the equivalent mass-spring system

$$\omega_{n1}^2 = \frac{\mu_j k_j + 0.5 m_j (k_j + s_j) - \sqrt{[\mu_j k_j + 0.5 m_j (k_j + s_j)]^2 - 2 m_j \mu_j k_j s_j}}{m_j \mu_j}, \tag{24}$$

$$\omega_{n2}^2 = \frac{\mu_j k_j + 0.5 m_j (k_j + s_j) + \sqrt{[\mu_j k_j + 0.5 m_j (k_j + s_j)]^2 - 2 m_j \mu_j k_j s_j}}{m_j \mu_j}, \tag{25}$$

and the two modal frequencies of the anti-symmetric modes are given by

$$\omega_{n1}^2 = \frac{\mu_j k_j + 2(J_j / L_j^2)(k_j + s_j) - \sqrt{[\mu_j k_j + 2(J_j / L_j^2)(k_j + s_j)]^2 - 8(J_j / L_j^2)\mu_j k_j s_j}}{4\mu_j J_j / L_j^2}, \tag{26}$$

$$\omega_{n1}^2 = \frac{\mu_j k_j + 2(J_j / L_j^2)(k_j + s_j) + \sqrt{[\mu_j k_j + 2(J_j / L_j^2)(k_j + s_j)]^2 - 8(J_j / L_j^2)\mu_j k_j s_j}}{4\mu_j J_j / L_j^2}. \tag{27}$$

From Eq. (24) to Eq. (27) it can be seen that, when

$$J_j = \frac{1}{4} m_j L_j^2, \tag{28}$$

Eq. (26) becomes Eq. (24) and Eq. (27) becomes Eq. (25). From Eq. (24) and Eq. (25) it can be worked out that,

$$k_j = \frac{1}{2} m_j (\omega_{n1}^2 + \omega_{n2}^2 - \omega_{\text{anti}}^2), \tag{29}$$

$$s_j = \frac{\omega_{n1}^2 \omega_{n2}^2 k_j}{(\omega_{n1}^2 + \omega_{n2}^2 - \omega_{\text{anti}}^2)\omega_{\text{anti}}^2 - \omega_{n1}^2 \omega_{n2}^2}. \tag{30}$$

Therefore, for given m_j and L_j, from Eqs. (23), (28), (29) and (30) μ_j, J_j, k_j and s_j can be determined. The number of parameters to be determined for the equivalent multi-rigid body system reduces to $8N$-2. These parameters are m_1, L_1, c_{l1}, $c_{r1}, k_{\varphi 1}, c_{\varphi 1}$, d_{l1}, d_{r1}, m_2, L_2, c_{l2}, $c_{r2}, k_{\varphi 2}, c_{\varphi 2}$, d_{l2}, d_{r2}, …, m_N, L_N, c_{lN}, c_{rN}, d_{lN}, d_{rN}. To determine these parameters, at least a set of $8N$-2 equations are required. These equations can be established based on the receptances of the semi-infinite track at a number of properly selected frequencies.

The vertical displacement of the left end of the first rigid bar is denoted by $w_1(t)$ (directed downward) and the rotation angle of the jth bar is denoted by $\varphi_j(t)$ (directed clockwise). The vertical displacement of the left support mass and that of the right support mass are denoted by $w_{lj}(t)$ and $w_{rj}(t)$ (directed downward). It can be seen that the equivalent system has $3N$+1 degrees of freedom

which are defined by $w_1(t), \varphi_1(t), \cdots, \varphi_N(t), w_{l1}(t), \cdots, w_{lN}(t), w_{r1}(t) \cdots, w_{rN}(t)$. The vector formed by them is also denoted by $\mathbf{q}_e(t)$, i.e.,

$$\mathbf{q}_e(t) = (w_1(t), \varphi_1(t), \cdots, \varphi_N(t), w_{l1}(t), \cdots, w_{lN}(t), w_{r1}(t) \cdots, w_{rN}(t))^T . \quad (31)$$

With these degrees of freedom, the receptance matrix of the equivalent system associated with $w_1(t)$ and $\varphi_1(t)$ can be worked out (See Appendix B). By equating the receptance matrix to that of the semi-infinite track at a number, M, of pre-selected frequencies, a set of $6M$ nonlinear equations are formed from which and Eqs. (23, 28-30), all the parameters of the equivalent system can be determined.

The so-far best determined parameters of the equivalent system are for $N = 5$ (therefore, the number of unknown parameters is $8 \times 5 - 2 = 38$) and listed in Table 7. The pre-selected frequencies are 3, 15, 27, 87, 117, 167, 217, 243, 277, 327, 377, 427, 457, 489, 517, 567, 617, 800 Hz ($M = 18$ and the total number of the equations is 108). Again, since the number of degrees of freedom of the equivalent system is much limited while that of the semi-infinite track is unlimited, the parameters are quite different from bar to bar. The receptance of the equivalent system and that of the semi-infinite ballasted track are compared in Fig. 14 and Fig. 15. It can be seen that for frequencies up to about 750 Hz, the comparison is satisfactory.

Table 7. Parameters of the equivalent system.

No. of the bar	1	2	3	4	5
m (kg)	7.546	28.416	29.702	110.540	246.240
J (kg·m^2)	0.069	1.146	1.174	13.360	7.651
L (m)	0.191	0.402	0.398	0.695	0.353
k (N/m)	2.629×10^7	9.899×10^7	10.347×10^7	38.508×10^7	85.780×10^7
c_l (N·s/m)	0.000	6.112	102.754	855.838	9348.099
c_r (N·s/m)	4.760	33275.108	868.211	3024.097	37546.257
k_φ (N·m/rad)	1.337×10^7	0.650×10^7	1.103×10^7	0.347×10^7	
c_φ (N·m·s/rad)	1373.233	122.498	3126.892	16752.988	
μ (kg)	15.913	59.927	62.640	233.120	519.301
s (N/m)	1.801×10^7	4.071×10^7	4.255×10^7	15.836×10^7	35.277×10^7
d_l(N·s/m)	18894.294	10238.527	12485.843	14138.425	2556.605
d_r (N·s/m)	4124.971	10.122	41742.950	2555.712	14094.973

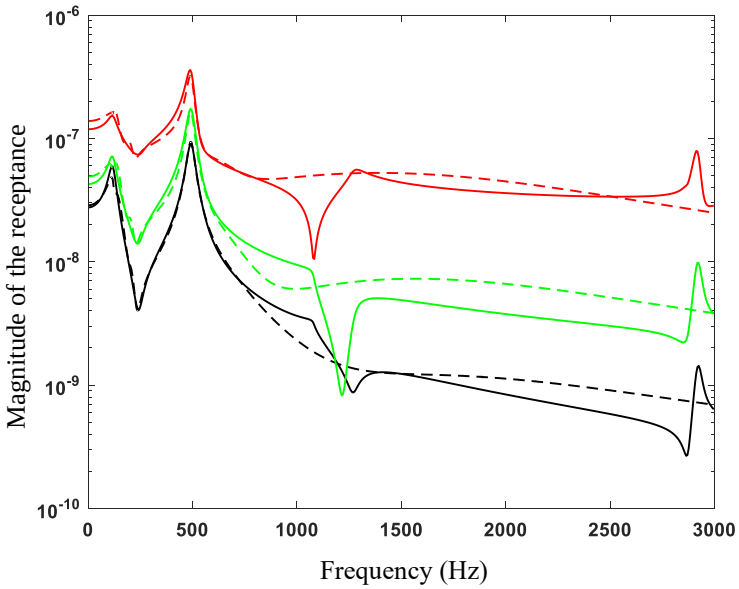

Fig. 14. The magnitudes of the receptances of the semi-ballasted track (—) and the equivalent system (- - -). Black for α_{11} (m/N), green for α_{12} (rad/N) and red for α_{22} (rad/(N·m))

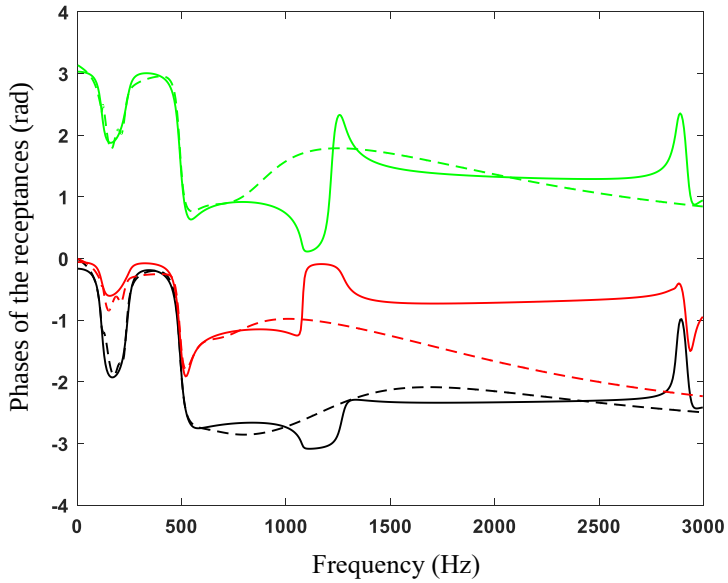

Fig. 15. The phases of the receptances of the semi-infinite ballasted track (—) and the equivalent system (- - -). Black for α_{11}, green for α_{12} and red for α_{22}

5.3 A preliminary validation of the equivalent multi-rigid body system

Rotating the multi-rigid body system shown in Fig. 12 about the left end by 180º produces a second multi-rigid body system. These two multi-rigid body systems joined together may be used to calculate the receptance of the complete track at the central cross-section for the frequency range in which the multi-rigid body system and the semi-infinite track are equivalent. The vertical receptance at the interface of the two multi-rigid body systems is shown in Fig. 16, in comparison with that of the complete track. It can be seen that for frequencies up to about 750 Hz, the comparison is satisfactory, although further improvement is still desirable.

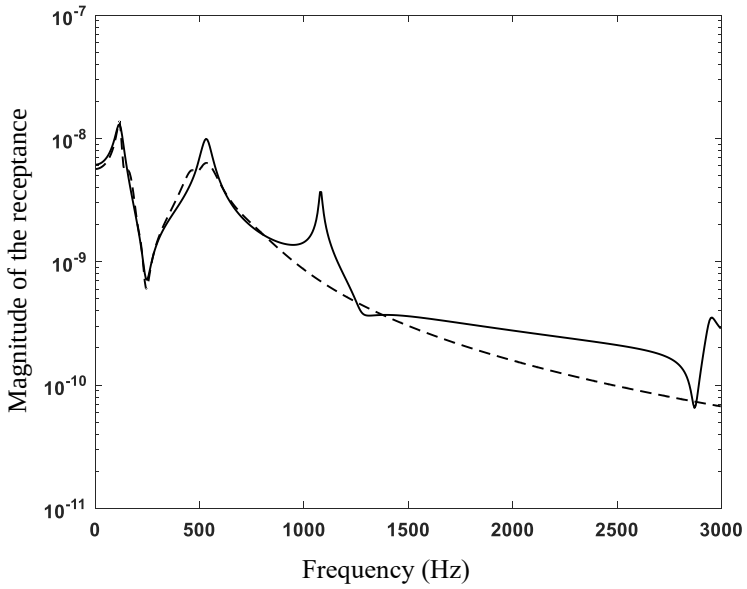

Fig. 16. The vertical receptance at the central cross-section of the complete ballasted track (—) and that at the interface of the two multi-rigid body systems (- - -)

6. Conclusion

In this paper, a method is proposed for calculating the receptance matrix of a semi-infinite periodic track and for determining a multi-rigid body system which is dynamically equivalent to the semi-infinite track. The receptance matrix is calculated based on two semi-infinite tracks joined together as a complete periodic structure subject to specific harmonic loads at the interface of the semi-infinite tracks, in combination with the relationship between the internal forces and displacements of a Timoshenko beam. Results are produced for the vertical vibration of a typical high-speed slab track and a typical ballasted track. Several vibration modes/frequencies are identified for the complete track: the bouncing mode/frequency, the pitching mode/frequency, the first pinned-pinned mode/frequency, the sliding-pinned-sliding* mode/frequency, the second pinned-pinned mode/frequency and the sliding-sliding*-sliding mode/frequency. For the ballasted track, there is an anti-resonance mode/frequency at which the sleeper behaves as a vibration absorber to the rail. The peaks/dips in the receptance of the semi-infinite track can be well explained based on the vibration modes or characteristics of the complete track.

The equivalent multi-rigid body system proposed in this paper is a train of rigid bars hinged together, geometrically looking like a rail. For the slab track, damped springs are present to support the bars at the ends, mimicking the fasteners. For the ballasted track, mass-spring-damper systems are present to support the bars at the ends, mimicking the fastener/sleeper/ballast systems. Damped bending springs are present to connect neighbouring bars, mimicking the bending stiffness of the rail. The parameters of the equivalent system are estimated by letting the modal frequencies of the equivalent multi-rigid body system be the same as the characteristic frequencies of the semi-infinite

track and by minimising the relative difference in receptance between the multi-rigid body system and the semi-infinite track at a set of pre-defined frequencies, including the characteristic frequencies of the semi-infinite track. The number of bars must be greater than 3, however, trial and error are needed to decide the best number of bars. It is turned that, since the number of degrees of freedom of the equivalent system is much limited while that of the semi-infinite track is unlimited, the parameters may be quite different from bar to bar.

It should be acknowledged that, in this paper the receptance matrix is determined only for vertical vibration of a semi-infinite track and the determined equivalent multi-rigid body system is valid only for frequencies lower than the first pinned-pinned frequency. Even for these frequencies, further improvement to the parameters is still desirable. The usefulness of the equivalent system in a truncated track model is still to be investigated. It seems to be a much more challenging problem to produce an equivalent system (including the structural layout and the determination of the associated parameters) for a frequency range large enough to include the pinned-pinned frequencies, even just for vertical vibration of the track. Nevertheless, the methodology presented in this paper may shed some light on the problem.

Acknowledgments

The authors acknowledge the support to this work from the National Natural Science Foundation of China (52272352) and Shanghai Foreign Experts Program (22WZ2506300).

Conflict of interest statement

We, the authors of this paper, certify that we have no affiliation with, or involvement in, any organisation or entity with any financial interest, or nonfinancial interest in the subject matter or materials discussed in this manuscript.

Appendix A. The mass, stiffness and damping matrices of the equivalent system of the slab track

The mass, stiffness and damping matrices of the equivalent system shown in Fig. 8 are derived here by expressing the kinetical and potential energies of the equivalent system and by expressing the virtual work done by the damping forces. To express the energies, the displacements of the rigid bars at the mass centres and the locations of the end springs should be expressed first. The vertical displacement of the kth bar at the left end is given by

$$w_{k1}(t) = w_1(t) + \sum_{j=1}^{k-1} \varphi_j(t) L_j \,, \tag{A.1}$$

or

$$\mathbf{w}_1(t) = \mathbf{A}_1 \mathbf{q}_e(t), \tag{A.2}$$

where $\mathbf{q}_e(t)$ is defined in Eq. (20),

$$\mathbf{w}_1(t) = (w_{11}(t), w_{21}(t), \cdots, w_{N1})^T, \tag{A.3}$$

and $\mathbf{A}_1$ is a matrix of order $N\times(N+1)$, given by

$$\mathbf{A}_1 = \begin{bmatrix} 1 & 0 & 0 & \cdots & \cdots & 0 & 0 \\ 1 & L_1 & 0 & \cdots & \cdots & 0 & 0 \\ 1 & L_1 & L_2 & \cdots & \cdots & 0 & 0 \\ \cdots & \cdots & \cdots & \cdots & \cdots & 0 & 0 \\ 1 & L_1 & L_2 & \cdots & L_{N-2} & 0 & 0 \\ 1 & L_1 & L_2 & \cdots & L_{N-2} & L_{N-1} & 0 \end{bmatrix}. \tag{A.4}$$

The vertical displacement of the kth bar at the mass centre is given by

$$w_{k0}(t) = w_1(t) + \sum_{j=1}^{k-1} \varphi_j(t) L_j + \frac{1}{2} \varphi_k(t) L_k, \tag{A.5}$$

or

$$\mathbf{w}_0(t) = \mathbf{A}_0 \mathbf{q}_e(t) \tag{A.6}$$

where

$$\mathbf{w}_0(t) = (w_{10}(t), w_{20}(t), \cdots, w_{N0})^T, \tag{A.7}$$

and $\mathbf{A}_0$ is a matrix of order $N\times(N+1)$, given by

$$\mathbf{A}_0 = \begin{bmatrix} 1 & 0.5L_1 & \cdots & \cdots & \cdots & 0 \\ 1 & L_1 & 0.5L_2 & \cdots & \cdots & 0 \\ 1 & L_1 & L_2 & 0.5L_3 & \cdots & 0 \\ \cdots & \cdots & \cdots & \cdots & \cdots & \cdots \\ 1 & L_1 & L_2 & \cdots & 0.5L_{N-1} & 0 \\ 1 & L_1 & L_2 & \cdots & L_{N-1} & 0.5L_N \end{bmatrix}. \tag{A.8}$$

The vertical displacement of the kth bar at the right end is given by

$$w_{k2}(t) = w_1(t) + \sum_{j=1}^{k} \varphi_j(t) L_j, \tag{A.9}$$

or

$$\mathbf{w}_2(t) = \mathbf{A}_2 \mathbf{q}_e(t), \tag{A.10}$$

where

$$\mathbf{w}_2(t)=(w_{12}(t),w_{22}(t),\cdots,w_{N2})^{\mathrm{T}}, \tag{A.11}$$

and $\mathbf{A}_2$ is a matrix of order $N\times(N+1)$, given by

$$\mathbf{A}_2=\begin{bmatrix}1 & L_1 & \cdots & \cdots & \cdots & 0\\ 1 & L_1 & L_2 & \cdots & \cdots & 0\\ 1 & L_1 & L_2 & L_3 & \cdots & 0\\ \cdots & \cdots & \cdots & \cdots & \cdots & \cdots\\ 1 & L_1 & L_2 & \cdots & L_{N-1} & 0\\ 1 & L_1 & L_2 & \cdots & L_{N-1} & L_N\end{bmatrix}. \tag{A.12}$$

The kinetic energy of the equivalent system is given by

$$\begin{aligned}T&=\sum_{j=1}^{N}\frac{1}{2}m_j\dot{w}_{j0}^2(t)+\sum_{j=1}^{N}\frac{1}{2}J_j\dot{\varphi}_j^2(t)\\&=\frac{1}{2}\dot{\mathbf{q}}_{\mathrm{e}}^{\mathrm{T}}(t)\mathbf{A}_0^{\mathrm{T}}\mathbf{M}'\mathbf{A}_0\dot{\mathbf{q}}_{\mathrm{e}}(t)+\frac{1}{2}\dot{\boldsymbol{\varphi}}^{\mathrm{T}}(t)\mathbf{J}\dot{\boldsymbol{\varphi}}(t),\\&=\frac{1}{2}\dot{\mathbf{q}}_{\mathrm{e}}^{\mathrm{T}}(t)\mathbf{M}_{\mathrm{e}}\dot{\mathbf{q}}_{\mathrm{e}}(t)\end{aligned} \tag{A.13}$$

where

$$\mathbf{M}'=\mathrm{diag}(m_1,m_2,\cdots,m_N), \tag{A.14}$$

$$\mathbf{J}=\mathrm{diag}(J_1,J_2,\cdots,J_N). \tag{A.15}$$

Therefore, the mass matrix of the equivalent system is

$$\mathbf{M}_{\mathrm{e}}=\mathbf{A}_0^{\mathrm{T}}\mathbf{M}'\mathbf{A}_0+\mathrm{diag}(0,\mathbf{J}). \tag{A.16}$$

The potential energy of the equivalent system is given by

$$\begin{aligned}U&=\sum_{j=1}^{N}\frac{1}{2}k_j w_{j1}^2(t)+\sum_{j=1}^{N}\frac{1}{2}k_j w_{j2}^2(t)+\sum_{j=1}^{N-1}\frac{1}{2}k_{\varphi j}[\varphi_{j+1}(t)-\varphi_j(t)]^2\\&=\frac{1}{2}\mathbf{q}^{\mathrm{T}}(t)\mathbf{A}_1^{\mathrm{T}}\mathbf{K}'\mathbf{A}_1\mathbf{q}_{\mathrm{e}}(t)+\frac{1}{2}\mathbf{q}_{\mathrm{e}}^{\mathrm{T}}(t)\mathbf{A}_2^{\mathrm{T}}\mathbf{K}'\mathbf{A}_2\mathbf{q}_{\mathrm{e}}(t)+\sum_{j=1}^{N-1}\frac{1}{2}k_{\varphi j}\varphi_{j+1}^2(t)+\sum_{j=1}^{N-1}\frac{1}{2}k_{\varphi j}\varphi_j^2(t)-\sum_{j=1}^{N-1}k_{\varphi j}\varphi_j(t)\varphi_{j+1}(t)\\&=\frac{1}{2}\mathbf{q}_{\mathrm{e}}^{\mathrm{T}}(t)\mathbf{A}_1^{\mathrm{T}}\mathbf{K}'\mathbf{A}_1\mathbf{q}_{\mathrm{e}}(t)+\frac{1}{2}\mathbf{q}_{\mathrm{e}}^{\mathrm{T}}(t)\mathbf{A}_2^{\mathrm{T}}\mathbf{K}'\mathbf{A}_2\mathbf{q}_{\mathrm{e}}(t)+\frac{1}{2}\boldsymbol{\varphi}^{\mathrm{T}}(t)\mathbf{K}'_{\varphi}\boldsymbol{\varphi}(t)+\frac{1}{2}\boldsymbol{\varphi}^{\mathrm{T}}(t)\mathbf{K}''_{\varphi}\boldsymbol{\varphi}(t)-\frac{1}{2}\boldsymbol{\varphi}^{\mathrm{T}}(t)\mathbf{K}'''_{\varphi}\boldsymbol{\varphi}(t)\end{aligned}$$

or

$$U=\frac{1}{2}\mathbf{q}_{\mathrm{e}}^{\mathrm{T}}(t)\mathbf{K}_{\mathrm{e}}\mathbf{q}_{\mathrm{e}}(t), \tag{A.17}$$

where

$$\mathbf{K}_{\mathrm{e}} = \mathbf{A}_1^{\mathrm{T}}\mathbf{K}'\mathbf{A}_1 + \mathbf{A}_2^{\mathrm{T}}\mathbf{K}'\mathbf{A}_2 + \mathrm{diag}(0, \mathbf{K}'_{\varphi} + \mathbf{K}''_{\varphi} - \mathbf{K}'''_{\varphi}), \tag{A.18}$$

is the stiffness matrix of the equivalent system, in which

$$\mathbf{K}' = \mathrm{diag}(k_1, k_2, \cdots, k_N), \tag{A.19}$$

$$\mathbf{K}'_{\varphi} = \mathrm{diag}(0, k_{\varphi 1}, k_{\varphi 2}, \cdots, k_{\varphi,N-1}), \tag{A.20}$$

$$\mathbf{K}''_{\varphi} = \mathrm{diag}(k_{\varphi 1}, k_{\varphi 2}, \cdots, k_{\varphi,N-1}, 0), \tag{A.21}$$

$$\mathbf{K}'''_{\varphi} = \begin{bmatrix} 0 & k_{\varphi 1} & \cdots & 0 \\ k_{\varphi 1} & 0 & \cdots & \cdots \\ \cdots & \cdots & 0 & k_{\varphi,N-1} \\ 0 & \cdots & k_{\varphi,N-1} & 0 \end{bmatrix}. \tag{A.22}$$

The virtual work done by the damping forces is given by (here δ means virtual displacement)

$$\begin{aligned} D &= -\sum_{j=1}^{N} c_{lj}\dot{w}_{j1}(t)\delta w_{j1} - \sum_{j=1}^{N} c_{rj}\dot{w}_{j2}(t)\delta w_{j2} - \sum_{j=1}^{N-1} c_{\varphi j}[\dot{\varphi}_{j+1}(t) - \dot{\varphi}_j(t)]\delta[\varphi_{j+1} - \varphi_j] \\ &= -\delta\mathbf{q}_{\mathrm{e}}^{\mathrm{T}}\mathbf{A}_1^{\mathrm{T}}\mathbf{C}'\mathbf{A}_1\dot{\mathbf{q}}_{\mathrm{e}}(t) - \delta\mathbf{q}_{\mathrm{e}}^{\mathrm{T}}\mathbf{A}_2^{\mathrm{T}}\mathbf{C}''\mathbf{A}_2\dot{\mathbf{q}}_{\mathrm{e}}(t) - \sum_{j=1}^{N-1} c_{\varphi j}\dot{\varphi}_{j+1}(t)\delta\varphi_{j+1} \\ &\quad - \sum_{j=1}^{N-1} c_{\varphi j}\dot{\varphi}_j(t)\delta\varphi_j + \sum_{j=1}^{N-1} c_{\varphi j}\dot{\varphi}_{j+1}(t)\delta\varphi_j + \sum_{j=1}^{N-1} c_{\varphi j}\dot{\varphi}_j(t)\delta\varphi_{j+1} \\ &= -\delta\mathbf{q}_{\mathrm{e}}^{\mathrm{T}}\mathbf{A}_1^{\mathrm{T}}\mathbf{C}'\mathbf{A}_1\dot{\mathbf{q}}_{\mathrm{e}}(t) - \delta\mathbf{q}_{\mathrm{e}}^{\mathrm{T}}\mathbf{A}_2^{\mathrm{T}}\mathbf{C}''\mathbf{A}_2\dot{\mathbf{q}}_{\mathrm{e}}(t) - \delta\boldsymbol{\varphi}^{\mathrm{T}}\mathbf{C}'_{\varphi}\dot{\boldsymbol{\varphi}}(t) - \delta\boldsymbol{\varphi}^{\mathrm{T}}\mathbf{C}''_{\varphi}\dot{\boldsymbol{\varphi}}(t) + \delta\boldsymbol{\varphi}^{\mathrm{T}}\mathbf{C}'''_{\varphi}\dot{\boldsymbol{\varphi}}(t) \end{aligned}$$

or

$$D = -\delta\mathbf{q}_{\mathrm{e}}^{\mathrm{T}}\mathbf{C}_{\mathrm{e}}\dot{\mathbf{q}}_{\mathrm{e}}(t), \tag{A.23}$$

where

$$\mathbf{C}_{\mathrm{e}} = \mathbf{A}_1^{\mathrm{T}}\mathbf{C}'\mathbf{A}_1 + \mathbf{A}_2^{\mathrm{T}}\mathbf{C}''\mathbf{A}_2 + \mathrm{diag}(0, \mathbf{C}'_{\varphi} + \mathbf{C}''_{\varphi} - \mathbf{C}'''_{\varphi}), \tag{A.24}$$

is the damping matrix of the equivalent system, and

$$\mathbf{C}' = \mathrm{diag}(c_{l1}, c_{l2}, \cdots, c_{lN}), \tag{A.25}$$

$$\mathbf{C}'' = \mathrm{diag}(c_{r1}, c_{r2}, \cdots, c_{rN}), \tag{A.26}$$

$$\mathbf{C}'_{\varphi} = \mathrm{diag}(0, c_{\varphi 1}, c_{\varphi 2}, \cdots, c_{\varphi,N-1}), \tag{A.27}$$

$$\mathbf{C}''_{\varphi} = \mathrm{diag}(c_{\varphi 1}, c_{\varphi 2}, \cdots, c_{\varphi,N-1}, 0), \tag{A.28}$$

$$\mathbf{C}_{\varphi}''' = \begin{bmatrix} 0 & c_{\varphi 1} & \cdots & 0 \\ c_{\varphi 1} & 0 & \cdots & \cdots \\ \cdots & \cdots & 0 & c_{\varphi,N-1} \\ 0 & \cdots & c_{\varphi,N-1} & 0 \end{bmatrix}. \tag{A.29}$$

Appendix B. The mass, stiffness and damping matrices of the equivalent system of the ballasted track

As in Appendix A, the mass, stiffness and damping matrices of the equivalent system are derived by expressing the kinetical and potential energies of the equivalent system and by expressing the virtual work done by the damping forces. To express the energies, the displacements of the rigid bars at the mass centres and the two ends should be expressed first. The vertical displacement of the *k*th bar at the left end is given by

$$w_{k1}(t) = w_1(t) + \sum_{j=1}^{k-1} \varphi_j(t) L_j \,, \tag{B.1}$$

or

$$\mathbf{w}_1(t) = \mathbf{B}_1 \mathbf{q}_e(t) \,, \tag{B.2}$$

where $\mathbf{q}_e(t)$ is defined in Eq. (31), $\mathbf{w}_1(t)$ is defined in Eq. (A.3) and $\mathbf{B}_1$ is of order $N \times (3N+1)$, given by

$$\mathbf{B}_1 = \begin{bmatrix} 1 & 0 & \cdots & \cdots & \cdots & 0 & \cdots & 0 \\ 1 & L_1 & 0 & \cdots & \cdots & 0 & \cdots & 0 \\ 1 & L_1 & L_2 & 0 & \cdots & 0 & \cdots & 0 \\ \cdots & \cdots & \cdots & \cdots & \cdots & \cdots & \cdots & \cdots \\ 1 & L_1 & L_2 & \cdots & L_{N-2} & 0 & \cdots & 0 \\ 1 & L_1 & L_2 & \cdots & L_{N-2} & L_{N-1} & \cdots & 0 \end{bmatrix}. \tag{B.3}$$

The vertical displacement of the *k*th bar at the mass centre is given by

$$w_{k0}(t) = w_1(t) + \sum_{j=1}^{k-1} \varphi_j(t) L_j + \frac{1}{2} \varphi_k(t) L_k \,, \tag{B.4}$$

or

$$\mathbf{w}_0(t) = \mathbf{B}_0 \mathbf{q}_e(t) \tag{B.5}$$

where $\mathbf{w}_0(t)$ is defined in Eq. (A.7) and $\mathbf{B}_0$ is of order $N \times (3N+1)$, given by

$$\mathbf{B}_0=\begin{bmatrix}1 & 0.5L_1 & 0 & 0 & \cdots & 0 & 0 & \cdots & 0\\ 1 & L_1 & 0.5L_2 & 0 & \cdots & 0 & 0 & \cdots & 0\\ 1 & L_1 & L_2 & 0.5L_3 & \cdots & 0 & 0 & \cdots & 0\\ \cdots & \cdots & \cdots & \cdots & \cdots & 0 & 0 & \cdots & 0\\ 1 & L_1 & L_2 & L_3 & \cdots & 0.5L_{N-1} & 0 & \cdots & 0\\ 1 & L_1 & L_2 & L_3 & \cdots & L_{N-1} & 0.5L_N & \cdots & 0\end{bmatrix}. \tag{B.6}$$

The vertical displacement of the kth bar at the right end is given by

$$w_{k2}(t)=w_1(t)+\sum_{j=1}^{k}\varphi_j(t)L_j\,, \tag{B.7}$$

or

$$\mathbf{w}_2(t)=\mathbf{B}_2\mathbf{q}_{\mathrm{e}}(t)\,, \tag{B.8}$$

where $\mathbf{w}_2(t)$ is defined in Eq. (A.11) and $\mathbf{B}_2$ is of order $N\times(3N+1)$ and given by

$$\mathbf{B}_2=\begin{bmatrix}1 & L_1 & 0 & 0 & \cdots & 0 & 0 & \cdots & 0\\ 1 & L_1 & L_2 & 0 & \cdots & 0 & 0 & \cdots & 0\\ 1 & L_1 & L_2 & L_3 & \cdots & 0 & 0 & \cdots & 0\\ \cdots & \cdots & \cdots & \cdots & \cdots & 0 & 0 & \cdots & 0\\ 1 & L_1 & L_2 & L_3 & \cdots & L_{N-1} & 0 & \cdots & 0\\ 1 & L_1 & L_2 & L_3 & \cdots & L_{N-1} & L_N & \cdots & 0\end{bmatrix}. \tag{B.9}$$

The vector formed by the displacements of the left support masses and that by the displacements of the right support masses are given by

$$\mathbf{w}_l(t)=(w_{l1}(t),w_{l2}(t),\cdots,w_{lN}(t))^{\mathrm{T}}=\mathbf{B}_l\mathbf{q}_e(t)\,, \tag{B.10}$$

$$\mathbf{w}_r(t)=(w_{r1}(t),w_{r2}(t),\cdots,w_{rN}(t))^{\mathrm{T}}=\mathbf{B}_r\mathbf{q}_{\mathrm{e}}(t)\,, \tag{B.11}$$

where ($\mathbf{E}$ is identity matrix)

$$\mathbf{B}_l=[\mathbf{0}_{N\times(N+1)},\mathbf{E}_{N\times N},\mathbf{0}_{N\times N}],\ \ \mathbf{B}_r=[\mathbf{0}_{N\times(N+1)},\mathbf{0}_{N\times N},\mathbf{E}_{N\times N}]. \tag{B.12}$$

The kinetic energy of the equivalent system is given by

$$\begin{aligned}T&=\sum_{j=1}^{N}\frac{1}{2}m_j\dot{w}_{j0}^2(t)+\sum_{j=1}^{N}\frac{1}{2}J_j\dot{\varphi}_j^2(t)+\sum_{j=1}^{N}\frac{1}{2}\mu_j\dot{w}_{lj}^2(t)+\sum_{j=1}^{N}\frac{1}{2}\mu_j\dot{w}_{rj}^2(t)\\&=\frac{1}{2}\dot{\mathbf{q}}_{\mathrm{e}}^{\mathrm{T}}(t)\mathbf{B}_0^{\mathrm{T}}\mathbf{M}'\mathbf{B}_0\dot{\mathbf{q}}_{\mathrm{e}}(t)+\frac{1}{2}\dot{\boldsymbol{\varphi}}^{\mathrm{T}}(t)\mathbf{J}\dot{\boldsymbol{\varphi}}(t)+\frac{1}{2}\dot{\mathbf{w}}_l^{\mathrm{T}}(t)\boldsymbol{\mu}\dot{\mathbf{w}}_l(t)+\frac{1}{2}\dot{\mathbf{w}}_r^{\mathrm{T}}(t)\boldsymbol{\mu}\dot{\mathbf{w}}_r(t)\,,\\&=\frac{1}{2}\dot{\mathbf{q}}_{\mathrm{e}}^{\mathrm{T}}(t)\mathbf{M}_{\mathrm{e}}\dot{\mathbf{q}}_{\mathrm{e}}(t)\end{aligned} \tag{B.13}$$

where $\mathbf{M}'$ and $\mathbf{J}$ are given by Eq. (A.14) and Eq. (A.15),

$$\boldsymbol{\mu} = \mathrm{diag}(\mu_1, \mu_2, \cdots, \mu_N)\,. \tag{B.14}$$

Therefore, the mass matrix of the equivalent system is

$$\mathbf{M}_\mathrm{e} = \mathbf{B}_0^\mathrm{T}\mathbf{M}'\mathbf{B}_0 + \mathrm{diag}(0, \mathbf{J}, \boldsymbol{\mu}, \boldsymbol{\mu})\,. \tag{B.15}$$

The potential energy of the equivalent system is given by

$$\begin{aligned} U &= \sum_{j=1}^{N}\frac{1}{2}k_j[w_{j1}(t) - w_{lj}(t)]^2 + \sum_{j=1}^{N}\frac{1}{2}s_j w_{lj}^2(t) + \sum_{j=1}^{N}\frac{1}{2}k_j[w_{j2}(t) - w_{rj}(t)]^2 \\ &\quad + \sum_{j=1}^{N}\frac{1}{2}s_j w_{rj}^2(t) + \sum_{j=1}^{N-1}\frac{1}{2}k_{\varphi j}[\varphi_{j+1}(t) - \varphi_j(t)]^2 \\ &= \sum_{j=1}^{N}\frac{1}{2}k_j w_{j1}^2(t) + \sum_{j=1}^{N}\frac{1}{2}(k_j + s_j)w_{lj}^2(t) - \sum_{j=1}^{N}k_j w_{j1}(t)w_{lj}(t) \\ &\quad + \sum_{j=1}^{N}\frac{1}{2}k_j w_{j2}^2(t) + \sum_{j=1}^{N}\frac{1}{2}(k_j + s_j)w_{rj}^2(t) - \sum_{j=1}^{N}k_j w_{j2}(t)w_{rj}(t) \\ &\quad + \sum_{j=1}^{N-1}\frac{1}{2}k_{\varphi j}\varphi_{j+1}^2(t) + \sum_{j=1}^{N-1}\frac{1}{2}k_{\varphi j}\varphi_j^2(t) - \sum_{j=1}^{N-1}k_{\varphi j}\varphi_j(t)\varphi_{j+1}(t) \end{aligned}\,. \tag{B.16}$$

In matrix form,

$$\begin{aligned} U &= \frac{1}{2}\mathbf{q}_\mathrm{e}^\mathrm{T}(t)\mathbf{B}_1^\mathrm{T}\mathbf{K}'\mathbf{B}_1\mathbf{q}_\mathrm{e}(t) + \frac{1}{2}\mathbf{q}_\mathrm{e}^\mathrm{T}(t)\mathbf{B}_l^\mathrm{T}\mathbf{K}''\mathbf{B}_l\mathbf{q}_\mathrm{e}(t) \\ &\quad - \frac{1}{2}\mathbf{q}_\mathrm{e}^\mathrm{T}(t)\mathbf{B}_1^\mathrm{T}\mathbf{K}'\mathbf{B}_l\mathbf{q}_\mathrm{e}(t) - \frac{1}{2}\mathbf{q}_\mathrm{e}^\mathrm{T}(t)\mathbf{B}_l^\mathrm{T}\mathbf{K}'\mathbf{B}_1\mathbf{q}_\mathrm{e}(t) \\ &\quad + \frac{1}{2}\mathbf{q}_\mathrm{e}^\mathrm{T}(t)\mathbf{B}_2^\mathrm{T}\mathbf{K}'\mathbf{B}_2\mathbf{q}_\mathrm{e}(t) + \frac{1}{2}\mathbf{q}_\mathrm{e}^\mathrm{T}(t)\mathbf{B}_r^\mathrm{T}\mathbf{K}''\mathbf{B}_r\mathbf{q}_\mathrm{e}(t) \\ &\quad - \frac{1}{2}\mathbf{q}_\mathrm{e}^\mathrm{T}(t)\mathbf{B}_2^\mathrm{T}\mathbf{K}'\mathbf{B}_r\mathbf{q}_\mathrm{e}(t) - \frac{1}{2}\mathbf{q}_\mathrm{e}^\mathrm{T}(t)\mathbf{B}_r^\mathrm{T}\mathbf{K}'\mathbf{B}_2\mathbf{q}_\mathrm{e}(t) \\ &\quad + \frac{1}{2}\boldsymbol{\varphi}^\mathrm{T}(t)\mathbf{K}'_\varphi\boldsymbol{\varphi}(t) + \frac{1}{2}\boldsymbol{\varphi}^\mathrm{T}(t)\mathbf{K}''_\varphi\boldsymbol{\varphi}(t) - \frac{1}{2}\boldsymbol{\varphi}^\mathrm{T}(t)\mathbf{K}'''_\varphi\boldsymbol{\varphi}(t) \end{aligned}\,, \tag{B.17}$$

where $\mathbf{K}'$, $\mathbf{K}'_\varphi$, $\mathbf{K}''_\varphi$ and $\mathbf{K}'''_\varphi$ are given by Eq. (A.19) to Eq. (A.22), while

$$\mathbf{K}'' = \mathrm{diag}(k_1 + s_1, k_2 + s_2, \cdots, k_N + s_N)\,. \tag{B.18}$$

Equation (B.17) can be written in a more compact form

$$U = \frac{1}{2}\mathbf{q}_\mathrm{e}^\mathrm{T}(t)\mathbf{K}_\mathrm{e}\mathbf{q}_\mathrm{e}(t)\,, \tag{B.19}$$

where

$$\begin{aligned}\mathbf{K}_{\mathrm{e}} &= \mathbf{B}_1^{\mathrm{T}}\mathbf{K}'\mathbf{B}_1 + \mathbf{B}_l^{\mathrm{T}}\mathbf{K}''\mathbf{B}_l - \mathbf{B}_1^{\mathrm{T}}\mathbf{K}'\mathbf{B}_l - \mathbf{B}_l^{\mathrm{T}}\mathbf{K}'\mathbf{B}_1 \\ &\quad + \mathbf{B}_2^{\mathrm{T}}\mathbf{K}'\mathbf{B}_2 + \mathbf{B}_r^{\mathrm{T}}\mathbf{K}''\mathbf{B}_r - \mathbf{B}_2^{\mathrm{T}}\mathbf{K}'\mathbf{B}_r - \mathbf{B}_r^{\mathrm{T}}\mathbf{K}'\mathbf{B}_2, \\ &\quad + \mathrm{diag}(0, \mathbf{K}'_\varphi + \mathbf{K}''_\varphi - \mathbf{K}'''_\varphi, \mathbf{0}_{N\times N}, \mathbf{0}_{N\times N})\end{aligned} \tag{B.20}$$

is the stiffness matrix of the equivalent system,

The virtual work done by the damping forces is given by (here δ means virtual displacement)

$$\begin{aligned}D &= -\sum_{j=1}^{N} c_{lj}(\dot{w}_{j1} - \dot{w}_{lj})\delta(w_{j1} - w_{lj}) - \sum_{j=1}^{N} d_{lj}\dot{w}_{lj}\delta w_{lj} \\ &\quad -\sum_{j=1}^{N} c_{rj}(\dot{w}_{j2} - \dot{w}_{rj})\delta(w_{j2} - w_{rj}) - \sum_{j=1}^{N} d_{rj}\dot{w}_{rj}\delta w_{rj} \\ &\quad -\sum_{j=1}^{N-1} c_{\varphi j}(\dot{\varphi}_{j+1} - \dot{\varphi}_j)\delta(\varphi_{j+1} - \varphi_j) \\ &= -\sum_{j=1}^{N} c_{lj}\dot{w}_{j1}\delta w_{j1} - \sum_{j=1}^{N}(c_{lj} + d_{lj})\dot{w}_{lj}\delta w_{lj} + \sum_{j=1}^{N} c_{lj}\dot{w}_{j1}\delta w_{lj} + \sum_{j=1}^{N} c_{lj}\dot{w}_{lj}\delta w_{j1} \\ &\quad -\sum_{j=1}^{N} c_{rj}\dot{w}_{j2}\delta w_{j2} - \sum_{j=1}^{N}(c_{rj} + d_{rj})\dot{w}_{rj}\delta w_{rj} + \sum_{j=1}^{N} c_{rj}\dot{w}_{j2}\delta w_{rj} + \sum_{j=1}^{N} c_{rj}\dot{w}_{rj}\delta w_{j2} \\ &\quad -\sum_{j=1}^{N-1} c_{\varphi j}\dot{\varphi}_{j+1}\delta\varphi_{j+1} - \sum_{j=1}^{N-1} c_{\varphi j}\dot{\varphi}_j\delta\varphi_j + \sum_{j=1}^{N-1} c_{\varphi j}\dot{\varphi}_{j+1}\delta\varphi_j + \sum_{j=1}^{N-1} c_{\varphi j}\dot{\varphi}_j\delta\varphi_{j+1}\end{aligned} \tag{B.21}$$

Or

$$\begin{aligned}D &= -\delta\mathbf{q}_{\mathrm{e}}^{\mathrm{T}}\mathbf{B}_1^{\mathrm{T}}\mathbf{C}'\mathbf{B}_1\dot{\mathbf{q}}_{\mathrm{e}}(t) - \delta\mathbf{q}_{\mathrm{e}}^{\mathrm{T}}\mathbf{B}_l^{\mathrm{T}}\mathbf{D}'\mathbf{B}_l\dot{\mathbf{q}}_{\mathrm{e}}(t) + \delta\mathbf{q}_{\mathrm{e}}^{\mathrm{T}}\mathbf{B}_l^{\mathrm{T}}\mathbf{C}'\mathbf{B}_1\dot{\mathbf{q}}_{\mathrm{e}}(t) + \delta\mathbf{q}_{\mathrm{e}}^{\mathrm{T}}\mathbf{B}_1^{\mathrm{T}}\mathbf{C}'\mathbf{B}_l\dot{\mathbf{q}}_{\mathrm{e}}(t) \\ &\quad -\delta\mathbf{q}_{\mathrm{e}}^{\mathrm{T}}\mathbf{B}_2^{\mathrm{T}}\mathbf{C}''\mathbf{B}_2\dot{\mathbf{q}}_{\mathrm{e}}(t) - \delta\mathbf{q}_{\mathrm{e}}^{\mathrm{T}}\mathbf{B}_r^{\mathrm{T}}\mathbf{D}''\mathbf{B}_r\dot{\mathbf{q}}_{\mathrm{e}}(t) + \delta\mathbf{q}_{\mathrm{e}}^{\mathrm{T}}\mathbf{B}_r^{\mathrm{T}}\mathbf{C}''\mathbf{B}_2\dot{\mathbf{q}}_{\mathrm{e}}(t) + \delta\mathbf{q}_{\mathrm{e}}^{\mathrm{T}}\mathbf{B}_2^{\mathrm{T}}\mathbf{C}''\mathbf{B}_r\dot{\mathbf{q}}_{\mathrm{e}}(t) \\ &\quad -\delta\boldsymbol{\varphi}^{\mathrm{T}}\mathbf{C}'_\varphi\dot{\boldsymbol{\varphi}}(t) - \delta\boldsymbol{\varphi}^{\mathrm{T}}\mathbf{C}''_\varphi\dot{\boldsymbol{\varphi}}(t) + \delta\boldsymbol{\varphi}^{\mathrm{T}}\mathbf{C}'''_\varphi\dot{\boldsymbol{\varphi}}(t)\end{aligned} \tag{B.22}$$

where $\mathbf{C}'$, $\mathbf{C}''$, $\mathbf{C}'_\varphi$, $\mathbf{C}''_\varphi$ and $\mathbf{C}'''_\varphi$ are given by Eq. (A.25)-Eq. (A.29), while

$$\mathbf{D}' = \mathrm{diag}(c_{l1} + d_{l1}, c_{l2} + d_{l2}, \cdots, c_{lN} + d_{lN}), \tag{B.23}$$

$$\mathbf{D}'' = \mathrm{diag}(c_{r1} + d_{r1}, c_{r2} + d_{r2}, \cdots, c_{rN} + d_{rN}). \tag{B.24}$$

Equation (B.22) may be written alternatively as

$$D = -\delta\mathbf{q}_{\mathrm{e}}^{\mathrm{T}}\mathbf{C}_{\mathrm{e}}\dot{\mathbf{q}}_{\mathrm{e}}(t), \tag{B.25}$$

where

$$\begin{aligned}\mathbf{C}_{\mathrm{e}} &= \mathbf{B}_1^{\mathrm{T}}\mathbf{C}'\mathbf{B}_1 + \mathbf{B}_l^{\mathrm{T}}\mathbf{D}'\mathbf{B}_l - \mathbf{B}_l^{\mathrm{T}}\mathbf{C}'\mathbf{B}_1 - \mathbf{B}_1^{\mathrm{T}}\mathbf{C}'\mathbf{B}_l \\ &\quad + \mathbf{B}_2^{\mathrm{T}}\mathbf{C}''\mathbf{B}_2 + \mathbf{B}_r^{\mathrm{T}}\mathbf{D}''\mathbf{B}_r - \mathbf{B}_r^{\mathrm{T}}\mathbf{C}''\mathbf{B}_2 - \mathbf{B}_2^{\mathrm{T}}\mathbf{C}''\mathbf{B}_r, \\ &\quad + \mathrm{diag}(0, \mathbf{C}'_\varphi + \mathbf{C}''_\varphi - \mathbf{C}'''_\varphi, \mathbf{0}_{N\times N}, \mathbf{0}_{N\times N})\end{aligned} \tag{B.26}$$

is the damping matrix of the equivalent system.

References

[1] X. Jin, Key problems faced in high-speed train operation, Journal of Zhejiang University Science A 15 (12) (2014) 936–945.

[2] J. C. O. Nielsen, A. Igeland, Vertical dynamic interaction between train and track-influence of wheel and track imperfections, Journal of Sound and Vibration 185 (1995) 825–839.

[3] A. Pieringer, W. Kropp, Model-based estimation of rail roughness from axle box acceleration, Applied Acoustics 193 (2022) 108760.

[4] L. Baeza, H. Ouyang, A railway track dynamics model based on modal sub-structuring and a cyclic boundary condition, Journal of Sound and Vibration 330 (1) (2011) 75-86.

[5] F. Dai, D. J. Thompson, Y. Zhu, X. Liu, Vibration properties of slab track installed on a viaduct, Proceedings of IMechE Part F: Journal of Rail and Rapid Transit 23(1) (2016) 235–252.

[6] S. Lei, Y. Ge, Q. Li, D. J. Thompson, Wave interference in railway track due to multiple wheels, Journal of Sound and Vibration 530 (2022) 116620.

[7] X. Zhao, Z. Wen, H. Wang, X. Jin, M. Zhu, Modelling of high-speed wheel-rail rolling contact on a corrugated rail and corrugation development, Journal of Zhejiang University Science A 15(12) (2014) 946-963.

[8] P. Dec, R. Cottereau, B. Faure, Introducing a moving load in a simulation in time over a truncated unbounded domain, Journal of Sound and Vibration 534 (2022) 117035.

[9] X. Sheng, C. J. C. Jones, D. J. Thompson, Responses of infinite periodic structures to moving or stationary harmonic loads, Journal of Sound and Vibration 282 (2005) 125-149.

[10] T. Mazilu, Green's functions for analysis of dynamic response of wheel/rail to vertical excitation, Journal of Sound and Vibration 306 (2007) 31–58.

[11] X. Sheng, Generalization of the Fourier transform-based method for calculating the response of a periodic railway track subject to a moving harmonic load, Journal of Modern Transportation 23 (2015) 12-29.

[12] X. Sheng, T. Zhong, Y. Li, Vibration and sound radiation of slab high-speed railway tracks subject to a moving harmonic load, Journal of Sound and Vibration 395 (2017) 160–186.

[13] X. Zhang, D. J. Thompson, Q. Li, D. M. Kostovasilis, G. R. Toward, G. Squicciarini, J. Ryue, A model of a discretely supported railway track based on a 2.5D finite element approach, Journal of Sound and Vibration 438 (2019) 153-174.

[14] X. Sheng, M. Li, C. J. C. Jones, D. J. Thompson, Using the Fourier-series approach to study interactions between moving wheels and a periodically supported rail, Journal of Sound and

Vibration 303 (2007) 873-894.

[15] T. Mazilu, M. Dumitriu, C. Tudorache, M. Sebeşan, Using the Green's functions method to study wheelset/ballasted track vertical interaction, Mathematical and Computer Modelling 54 (1-2) (2011) 261-279.

[16] T. Mazilu, Interaction between moving tandem wheels and an infinite rail with periodic supports – Green's matrices of the track method in stationary reference frame, Journal of Sound and Vibration 401 (2017) 233-254.

[17] X. Sheng, X. Xiao, S. Zhang, The time-domain moving Green function of a railway track and its application to wheel–rail interactions, Journal of Sound and Vibration 377 (2016) 133-154.

[18] S. Zhang, G. Cheng, X. Sheng, D. J. Thompson, Dynamic wheel-rail interaction at high speed based on time-domain moving Green's functions, Journal of Sound and Vibration 488 (2020) 115632.

[19] X. Xiao, X. Jin, Z. Wen, Effect of disabled fastening systems and ballast on vehicle derailment, Journal of Vibration and Acoustics 129 (2007) 217-229.

[20] S. Song, W. Zhang, P. Han, D. Zou, Sliding window method for vehicles moving on a long track, Vehicle System Dynamics 56(1) (2018) 113-127.

[21] J. Yang, D. J. Thompson, A non-reflecting boundary for use in a finite element beam model of a railway track, Journal of Sound and Vibration 337 (2015) 199-217.

[22] V. Krylov, F. Tilman, Acoustic 'black holes' for flexural waves as effective vibration dampers, Journal of Sound and Vibration 274 (2004) 605-619.

[23] L. Zhang, X. Sheng, A review on the research progress of mechanical meta-structures and their applications in rail transit, Intelligent Transportation Infrastructure 1 (2022) liac010.

[24] U. Basu, A. Chopra, Perfectly matched layers for time-harmonic elastodynamics of unbounded domains: theory and finite-element implementation. Computer Methods in Applied Mechanics and Engineering 192 (11–12) (2003) 1337–1375.

[25] U. Basu, A. Chopra, Perfectly matched layers for transient elastodynamics of unbounded domains, International Journal for Numerical Methods in Engineering 59 (2004) 1039–1045.

[26] U. Basu, A. Chopra, Erratum to 'perfectly matched layers for transient elastodynamics of unbounded domains', International Journal for Numerical Methods in Engineering 61 (2004) 156–157.

[27] M. Schill, Damped second-order Rayleigh-Timoshenko semi-infinite beam vibration—an exact complex dynamic member stiffness matrix, International Journal for Numerical Methods in Engineering 26(8) (1988) 1893-905.

[28] Y-H. Chen, Y-H. Huang, C.-T. Shih, Response of an infinite Timoshenko beam on a viscoelastic foundation to a harmonic moving load, Journal of Sound and Vibration 241(5) (2001) 809-824.

[29] K. Abe, S. Fujishita, K. Koro, Development of transmitting boundary for periodically supported rails, Journal of Mechanical Systems for Transportation and Logistics 3 (2010) 44-52.

[30] X. Zhang, D. J. Thompson, X. Sheng, Differences between Euler-Bernoulli and Timoshenko beam formulations for calculating the effects of moving loads on a periodically supported beam, Journal of Sound and Vibration 481 (2020) 115432.

[31] K. F. Graff, Wave Motion in Elastic Solids, Dover Publications, New York, 1991.

[32] X. Sheng, M. H. Li, Propagation constants of railway tracks as a periodic structure, Journal of Sound and Vibration 299 (2007) 1114–1123.

A list of tables

Table 1. Continuity or discontinuity at x_0 where a point force or moment is applied

$w_1(x,t)$	$\psi_1(x,t)$	$\partial w_1(x,t)/\partial x$	$\partial \psi_1(x,t)/\partial x$
Continuous but not smooth	Continuous and smooth	step	Continuous but not smooth
$w_2(x,t)$	$\psi_2(x,t)$	$\partial w_2(x,t)/\partial x$	$\partial \psi_2(x,t)/\partial x$
Continuous and smooth	Continuous but not smooth	Continuous but not smooth	step

Table 2. Parameters for the vertical dynamics of the track

Density of the rail	ρ = 7850 kg/m^3
Young's modulus of the rail	$E = 2.1\times10^{11}$ N/m^2
Shear modulus of the rail	$G = 0.81\times10^{11}$ N/m^2
Loss factor of the rail	$\eta_R = 0.01$
Cross-sectional area of the rail	$A = 7.69\times10^{-3}$ m^2
Second moment of area of the rail	$I = 30.55\times10^{-6}$ m^4
Shear coefficient of the rail cross-section	$\kappa = 0.4$
Vertical rail pad stiffness	$k_v = 5.44\times10^7$ N/m
Rotational rail pad stiffness	$k_\varphi = 2.83\times10^5$ N·m/rad
Rail pad loss factor	$\eta_P = 0.1$
Fastener spacing	d = 0.65 m

Table 3. Vibration characteristics of the complete slab track

Peak or dip frequency (Hz)	Description of the mode
183	Rail bouncing on the stiffness of the fasteners
940	The first pinned-pinned mode
980	The sliding-pinned-sliding* mode
2577	The second pinned-pinned mode
2607	The sliding-sliding*-sliding mode

Table 4. Parameters of the mass-spring-damper system equivalent to the semi-slab track

No. of bar	1	2	3	4	5
m (kg)	10.080	0.000	67.013	0.000	257.134
J (kg·m^2)	0.021	0.000	3.104	0.000	0.917
L (m)	0.091	0.329	0.430	0.181	0.119
k (N/m)	0.666×10^7	0.000	4.430×10^7	0.000	16.998×10^7
c_l (N·s/m)	0.000	0.206×10^3	2.876×10^3	0.000	0.000
c_r (N·s/m)	0.206×10^3	2.876×10^3	0.000	0.000	102.930×10^3
k_φ (N·m/rad)	2.099×10^7	1.275×10^7	0.288×10^7	0.061×10^7	
c_φ (N·m·s/rad)	0.321×10^3	2.882×10^3	0.529×10^3	0.792×10^3	

Table 5. Parameters for the vertical dynamics of the ballasted track

Parameters for the rail	As in Table 2
Vertical rail pad stiffness	$k_v = 3.5\times10^8$ N/m
Rotational rail pad stiffness	$k_\varphi = 1.82\times10^6$ N·m/rad
Rail pad loss factor	$\eta_P = 0.1$
Mass of half a sleeper	$m_S = 150$ kg
Sleeper spacing	$d = 0.6$ m
Ballast stiffness	$k_B = 100\times10^6$ N/m
Ballast loss factor	$\eta_B = 0.3$

Table 6. Vibration characteristics of the complete ballasted track

Peak or dip frequency (Hz)	Description of the mode
117	Rail and sleeper bouncing together on the ballast
243	Sleeper behaving as vibration absorber to the rail
531	Rail and sleeper bouncing out-of-phase
1077	The first pinned-pinned mode
1269	The sliding-pinned-sliding* mode
2871	The second pinned-pinned mode
2955	The sliding-sliding*-sliding mode

Table 7. Parameters of the equivalent system.

No. of the bar	1	2	3	4	5
m (kg)	7.546	28.416	29.702	110.540	246.240
J (kg·m^2)	0.069	1.146	1.174	13.360	7.651
L (m)	0.191	0.402	0.398	0.695	0.353
k (N/m)	2.629×10^7	9.899×10^7	10.347×10^7	38.508×10^7	85.780×10^7
c_l (N·s/m)	0.000	6.112	102.754	855.838	9348.099
c_r (N·s/m)	4.760	33275.108	868.211	3024.097	37546.257
k_φ (N·m/rad)	1.337×10^7	0.650×10^7	1.103×10^7	0.347×10^7	
c_φ (N·m·s/rad)	1373.233	122.498	3126.892	16752.988	
μ (kg)	15.913	59.927	62.640	233.120	519.301
s (N/m)	1.801×10^7	4.071×10^7	4.255×10^7	15.836×10^7	35.277×10^7
d_l(N·s/m)	18894.294	10238.527	12485.843	14138.425	2556.605
d_r (N·s/m)	4124.971	10.122	41742.950	2555.712	14094.973

A list of figures